TOC

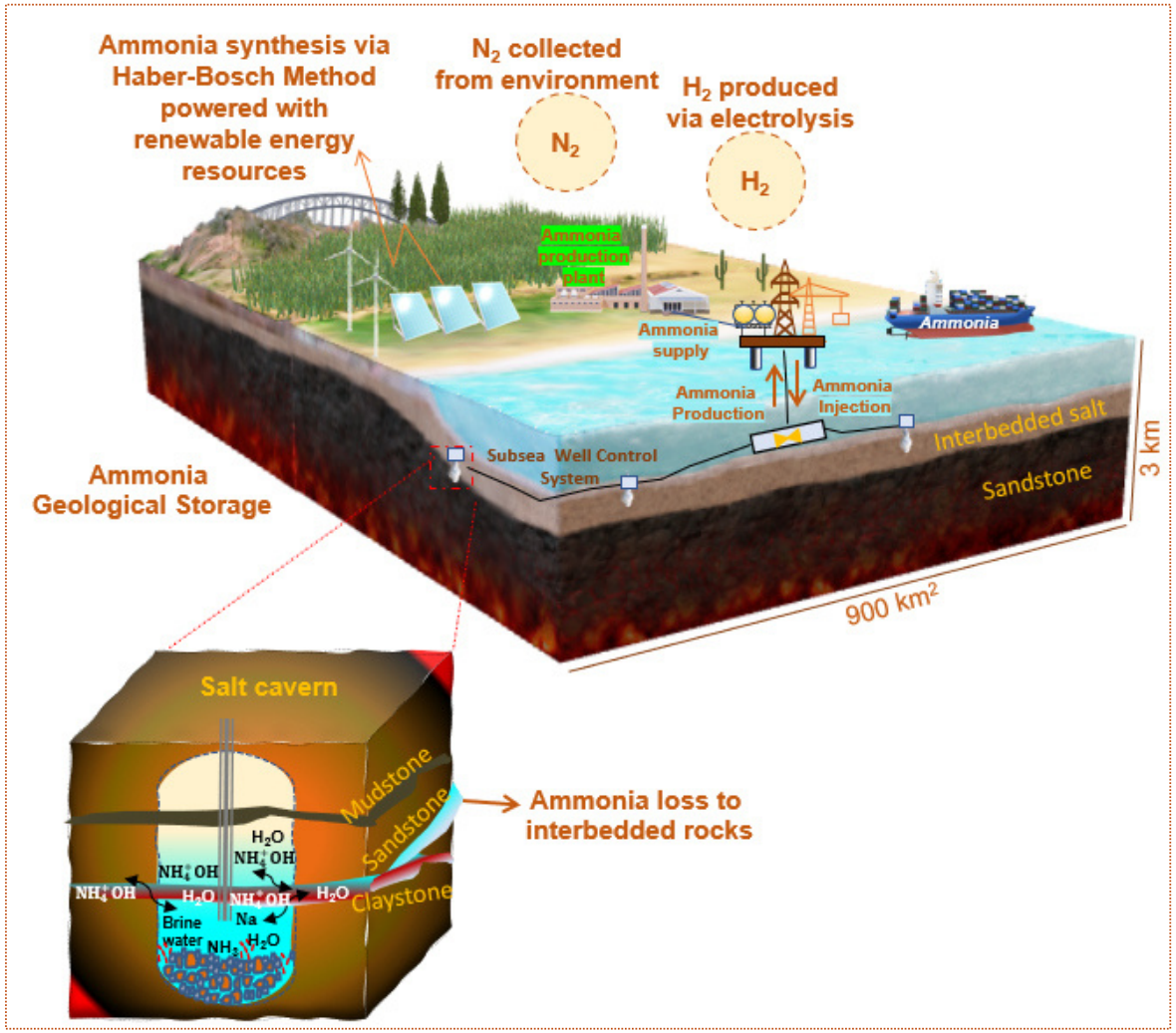
Ammonia synthesis via Haber-Bosch Method powered with renewable energy resources
N_2 collected from environment
N_2
H_2 produced via electrolysis
H_2
Ammonia production plant
Ammonia supply
Ammonia
Ammonia Production
Ammonia Injection
Subsea Well Control System
Interbedded salt
Sandstone
3 km
900 km^2
Ammonia Geological Storage
Salt cavern
Mudstone
Sandstone
Claystone
Ammonia loss to interbedded rocks
H_2O
NH_4^+ OH^-
Brine water
Na
NH_3

Unlocking Geological Hydrogen Storage with Ammonia: An Effort for Net-Zero Future

Adnan Aftab *Curtin University, Australia*
King Abdullah University of Science & Technology, Saudi Arabia

*Corresponding authors E-mail: *adnanaftab1199@gmail.com; adnan.aftab@curtin.edu.au*

This paper is non-peer reviewed preprint submitted to EarthArXiv. This paper has been not submitted anywhere for the publication. We should provide DOI of this paper once it would be published. The first author of this paper A. Aftab tweets @Nizamani1.

Abstract

Hydrogen gas (H_2) generation systems, comprising carbon capture and storage technology (CCST) play a crucial role to achieve the U.N. Net Zero goal before 2050. However, a critical challenge in grid-scale H_2 storage is the low volumetric energy density. One prospective approach is to use ammonia (NH_3) as a chemical carrier for H_2 and store it. This paper presents a state-of-the-art report on NH_3 and H_2 that details a variety of scientific challenges for their geological storage at reservoir conditions.

Keywords: Net Zero, H_2 carrier, NH_3 energy, hydrogeochemical, geological storage

Net Zero targets and hydrogen and ammonia

The need for a Net Zero environment is reshaping current energy sources in efforts to prevent the impact of global warming (Meys et al., 2021; Santamarina et al., 2022; Aftab et al, 2023). Burning fossil fuels account for more than 89% of atmospheric CO_2 emissions with 33 GT released in 2019 (EIA, 2019). Current temperatures are increasing by ~0.36 °C per decade (NASA, 2021; Ou et al., 2021; Ding et al, 2024) (Figure 1a). Consequently, these temperature increases could also result in adverse effects on humans, plants, animals, and ice sheets (EU, 2021; UN, 2021).

H_2 plays a central role in a Net Zero 2030 scenario with demand expected to increase between 73 to 158 Mt (Yusaf et al., 2022) (Figure 1b). A grid-scale H_2 energy system helps enable a Net Zero target by decarbonizing energy production, transport and long-term energy storage systems (Aftab et al., 2022; Cesaro et al., 2021; Espinoza and Santamarina, 2017). On a mass basis, H_2 has a high gravimetric energy density of ~141.86 MJ/kg which is 3 times the energy density of gasoline (Hassanpouryouzband et al., 2021). However, the volumetric energy density is low at 5.6 MJ/l (Krishnan Rajeshwar and Licht, 2008) compared to NH_3 which is 11.5 MJ/l (Nagaoka et al., 2017) at similar conditions of 1 atm and 20 °C as illustrated in Figure 2. Therefore, H_2 requires more extensive storage facilities and higher injection pressures than liquid NH_3 to ensure economical storage (Li et al., 2021). Typical liquid H_2 storage tanks operate between 340 to 680 atm which requires energy intensive cryogenic/refrigeration and insulation systems to facilitate transportation (Energy, 2021). Table 1 compares key physical and chemical properties of different fluids including water, NH_3, H_2, CH_4 and CO_2.

Table 1 Physical and chemical properties of water, ammonia, hydrogen, methane, and carbon dioxide.

Property	Water (H_2O)	Ammonia (NH_3)	Hydrogen (H_2)	Methane (CH_4)	Carbon dioxide (CO_2)	References
Molecular structure				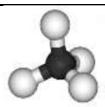	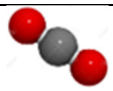	(NLM, 2022a)
Molecular weight (kg/mol)	18	17	2	16	44	
Color and odor	Colorless, odorless	Colorless, pungent smell	Colorless, odorless	Colorless, odorless	Colorless, odorless	

Volumetric energy densities (MJ/l)	0.001 Liquid	12 Liquid	10.1 Liquid 5.6 Compressed 0.0107 Ambient	22.2 Liquid 9 Compressed	NA	(IEA-AMP, 2022; Mazloomi and Gomes, 2012; Mogensen et al., 2019)
Gravimetric energy densities (MJ/kg)	0.001 Liquid	19 Liquid 0.4 Compressed	143 Liquid/ Compressed/ Ambient	53.6 Liquid/ Compressed/ Ambient	NA	
pH	7	~10.5 to 11.5	NA	NA	3.6	(Airgas, 2016; Johnson, 2019; USGS, 2019)
Specific gravity	1	0.60	0.07	0.56	1.53	(Gravities, 2022; Thermophysical, 2022)
Gas viscosity (cp)	NA	0.01	0.0089	0.01	0.015	(Council and Levels, 2008; Kapeghian et al., 1982; NLM, 2022b)
Liquid viscosity (cp)	0.89	0.127	0.0137	NA	0.0593	(Huber et al., 2009; Laesecke and Muzny, 2017; Leachman et al., 2009;

						Monogenidou et al., 2018)
Diffusivity in water (10^{-9} m^2/s)	NA	1.7, 2.0, 2.3	5.8, 4.4	2.4	1.96	(Arnold, 1930; Carlson, 1911; Davidson, 1957; Green and Perry, 2008; Moradi et al., 2020)
Vapor pressure (atm)	0.0311	8.571	~2.99	NA	NA	(Grilly, 1951; Perman, 1903; Speight, 2017)
Sound speed (m/s)	1496	433	1315	448	268	(Eric W. Lemmon, 2022)
Enthalpy (kJ/kg)	104	1692	3931	909	505	
Normal boiling point (˚C)	100	-33	-252	-161	-78	
Triple point temperature (˚C)	0.01	-77	-259	-182	-56	(Gravities, 2022; Thermophysical, 2022)
Triple point pressure (atm)	0.006	0.059	0.069	0.114	5.132	
Critical pressure (atm)	217	112	12	45	72	(Eric W. Lemmon, 2022)
Critical temperature (˚C)	374	132	-240	-82	31	
Critical density (kg/m^3)	322	233	31	162	467	

Gas density (kg/m^3)	NA	0.69	0.08	0.64	1.78	
Liquid density (kg/m^3)	997	603	14	NA	724	
Flammable limits in air (%)	NA	15 to 28	4 to 75	4 to 16	NA	(EngineeringTool, 2022; Flammability, 2022; Mazloomi and Gomes, 2012)
Autoignition temperature (˚C)	NA	630	585	540	NA	(Gummer and Hawksworth, 2008; INCHEM, 2022; Robinson and Smith, 1984)
Specific heat at constant pressure Cp (J/Kg˚C)	4137	2162	1430	2232	850	(Lemmon and Jacobsen, 2004)
Specific heat at constant volume Cv (J/kg˚C)	4181	1642.6	1018	1708	657	
Dipole moment (Coulomb meter)	6.187×10^{-30}	4.903×10^{-30}	NA	NA	NA	
Thermal conductivity (W/m*K)	0.60	0.02	0.18	0.03	0.01	

Solubility in water (%)	NA	42.8 to 52.9	0.00016	0.02	0.16	(Laby, 1986)

By contrast to pure H_2, NH_3 is a promising liquid chemical carrier for a sustainable grid-scale energy storage system with current production at 175 million tons/year and at a much lower cost. NH_3 easily liquifies through compression at 25 °C and 9.8 atm and has a 1.5 times higher volumetric energy density than liquid H_2 which compresses at -253 °C and 1 atm (Valera-Medina et al., 2018). However, NH_3 has 1/10th of the heat combustion capacity of H_2 (Kojima, 2014) which prevents the direct use of NH_3 in internal combustion engines (Koike et al., 2012). In addition, NH_3 is highly toxic with low flammability limits in air-yet the inverse is true for H_2 which is non-toxic and highly explosive (Karabeyoglu and Evans, 2012; Valera-Medina et al., 2018) (Figure S1). Despite these challenges, NH_3 contains appropriate thermophysical properties that favor in-situ geological storage conditions - namely the high volumetric energy density, high viscosity, less diffusivity, and high solubility in water in comparison to H_2 in water (Patonia and Poudineh, 2020; Santamarina et al., 2022).

Despite the known advantages of NH_3, there is a scarcity of data on its thermodynamic behavior, interaction with reservoir rocks and fluids, and required reservoir storage capacity, which are needed to develop grid-scale NH_3 geological storage facilities (Cesaro et al., 2021; Patonia and Poudineh, 2020).

Modeling tool and setups

The one-dimensional reactive mass transport modelling setup is the simulation software pH-REdox-EQuilibrium in the C programming language (PHREEQC) version 3. The software can

simulate chemical reactions and transport mechanisms in saltwater solution. The program uses equilibrium chemistry of aqueous solutions that react with solids, minerals, and gases. We have provided detail methodology of this work in the supplementary information.

Thermodynamics of ammonia and hydrogen at reservoir temperatures and pressures

NH_3 storage depends on accurate estimates of the physical properties and imbibition processes relative to the formation water saturation in porous media. The NH_3 density (ζ_{NH_3}) is > the H_2 density (ζ_{H_2}) and slightly increases with pressure and decreases with temperature, however, is still high in comparison to ζ_{H_2} (Kojima, 2014) (Figure 3a). The higher liquid NH_3 viscosity (μ_{NH_3}) prevents mobility within reservoir rocks (Figure 3b). However, the low H_2 viscosity (μ_{H_2}) can result in viscous fingering, increase the risk of loss within the pore network system, and high cushion gas pressure requirements that lead to geo-storage security risks (Iglauer, 2021).

Liquid NH_3 is highly water soluble due to its high density and consequently has less potential to negatively impact the sealing rock (Figure S2a). Cushion fluid (i.e., nitrogen gas) does not initiate viscous fingering for liquid NH_3 unlike in H_2 where residual methane as a cushion fluid could cause viscous fingering (Hassanpouryouzband et al., 2021). NH_3 added water solution surface tension decreases with an increase in NH_3 weight percent in water (Ware, 1928). Since NH_3 is surface active when compared to water thus NH_3 molecules move to the surface region and push water molecules to the inner side of the interface regions (Paul and Chandra, 2005). Consequently, a large amount of NH_3 molecules decrease water surface tension as determined by capillary height technique (Figure S2b). Moreover, water molecules in the inner side of NH_3 water interface tend to develop hydrogen bonds leading to higher values of water dipoles

relative to normal surface. The possible orientation of NH_3 molecules interface is outward due to dipole vector orientation relative to surface plane (Paul and Chandra, 2005). Moreover, the water molecules interfacial is oriented to inner side of the interface. The liquid-vapour interface thickness can be measured via variety of techniques such as fitting inconsistent density distribution behavior via error function (Senapati and Berkowitz, 2001), hyperbolic tangent function (Rowlinson and Widom, 2013) and change in the density over interface distance when compared to density of bulk liquid (Alejandre et al., 1995). Additionally, Figure S2b shows that thickness of NH_3 water interface layer increases after increasing the concentration of NH_3 in water. This increase in the thickness of interface layer occurs due to high volatility and weaker interaction of NH_3 molecules compared to water molecules which increases the NH_3 water interface layer. Thus, these findings show that surface tension and interface of NH_3 water layer can influence the NH_3 geological storage in the porous and permeable sedimentary formations. The outward orientation of NH_3 water interface may establish direct contact of NH_3 or NH_4^+OH with grains of the sedimentary rock and ensure hydrophobicity in the rock system leading to an increase in the wettability of NH_3 or NH_4^+OH on the rock surface and permanent NH_3 trapping hence the large amount of injected NH_3 can loss into the reservoir. Consequently, the reservoir rock may change from water-wet to NH_3-wet.

Hydrogeochemical behavior of liquid ammonia

NH_3 is very similar to water because of its solvent characteristics (Franklin and Kraus, 1899; Franklin, 1935). NH_3 molecules form weaker hydrogen bonds than water molecules due to the presence of nitrogen atoms and higher proton affinity leading to the ionization of NH_3 in water (Lagowski, 1978). For instance, sedimentary formations contain in-situ water or brine (Alemu et al., 2013). When liquid NH_3 mixes with water, it immediately gains H^+ ions from water to chemically transform NH_3 into ammonium ions (NH_4^+) ions and $OH^-_{(aq)}$ ions (Sanger and Danner, 2010) as illustrated in Equation 1.

$$NH_{3\,(aq)} + H_2O \longleftrightarrow NH_4^+OH_{(aq)} \longleftrightarrow NH_{4\,(aq)}^+ + OH^-_{(aq)} \qquad 1$$

NH_3 water solutions contain NH_3 molecules (alone or associated with neutral water molecules) or $NH_{4\,(aq)}^+$ and $OH^-_{(aq)}$ ions (Hadjipanayiotou et al., 1993; Sanger and Danner, 2010). Earlier research using XRD results (Bertie and Shehata, 1984), thermodynamic data (Yoke, 1991), Gaussian calculations (Hawkes, 2004), and spectroscopy findings (Price et al., 1991) conclude that NH_3/water solutions contain very minute amounts of $NH_{4\,(aq)}^+$ and $OH^-_{(aq)}$ ions and that NH_3 remains a major component.

Aqueous NH_3 has the potential to dissolve into the formation water and disperse through reservoir rock, which may have implications on injection/production loading cycles. The presence of NH_3 and NH_4^+OH could trigger hydrogeochemical interactions with reservoir rocks including shale (Patel et al., 2007), sandstone (Day and Huitt, 1967; Wang et al., 2011), and carbonate (Popescu et al., 2014). Aqua NH_3 or NH_4^+OH solutions react with several organic and inorganic acids to form ammonium salts, complexion salts (with certain metals), and haloamines (with halogens).

Liquid NH_3 interacts with montmorillonite and reduces the radius of the diffuse double layer in the clay which results in formation particle contraction, prevents swelling and slightly influences the permeability and hardness of the formation (Liu et al., 2015). In shales, NH_4^+OH ions combine with diffused cations on the surface of clay platelets and augment the Van der Waals forces between the formation sheets and protect the permeability of the reservoir (James and Harward, 1962). NH_3 replaces water molecules in the space between the clay sheets. This replacement implicates coordination of ammonium (NH_4^+OH) with exchangeable cations, in particular Ca^{2+} and Na^{2+}. These processes form NH_4^+ ions via protonation and physical adsorption of NH_3 in the interlayer spacing (James and Harward, 1962). Moreover, Fourier transform infrared studies indicate that NH_3-hydrogen bonding with oxygen and OH^- are very

weak in silicate sheets (Alshameri et al., 2018). X-ray diffraction data show 9.78 Å and 12.42 Å basal spacing for pristine montmorillonite and NH_3 treated montmorillonite, respectively (Sugahara et al., 2017). Therefore, a similar behavior would be expected for cap rock in reservoir if treated with NH_3. However, formation water, chemical ions and different mineral concentrations could influence the reservoir rock.

Sandstone adsorbs water and reduces the cementing strength between the grains which results in sandstone swelling and or softness (Figure S3a) (Day and Huitt, 1967). These processes reduce the permeability of the rock. Sandstone typically contains dolomite, kaolinite, and quartz minerals. When water reacts with these minerals, it forms montmorillonite due to partial degradation of the minerals and carbonate traces. The process of montmorillonite formation requires quartz and significantly increases in the presence of silica, dolomite, and kaolinite (Figure S3b). Consequently, the sandstone hardness increases due to mineral reorientation and recrystallization (Day and Huitt, 1967). NH_3 prevents sandstone swelling and does not alter the original grain orientation and morphology. Consequently, these factors may have a positive impact on the withdrawal of liquid NH_3 from geological reservoirs.

The important parameter that measures the proportion of $NH_3 \longrightarrow NH_4^+OH$ in water is pH (Erickson, 1985). Moreover, temperature and ionic strength influence the activity of NH_3 in water. High temperature increases the ionic concentration of the solution (i.e., 6.166 mol/kg at 25 °C to 6.348 mol/kg at 50 °C) and consequently decreases the pH (i.e., 12.7 at 25 °C to 11.6 at 50 °C) of system due to release of H^+. Therefore, this mechanism shifts equilibrium to left leading to formation of NH_3 however inverse is true for the generation of NH_4^+OH in equation 1 (Warren, 1962). Figure 4a shows that pH of Halite:Water (250 g:1 kg) solution increases to ~11.8 after addition of 170 g of NH_3. Once the pH>11, it converts all ammonium ions into molecular NH_3 (Bremner and Tabatabai, 1972).

We estimate the dissolution and precipitation behaviour of halite and anhydrite in the present of NH_3 brine solution to evaluate the possibility of NH_3 geological storage in the salt caverns. We determine concentrations of elements, activities of aqueous species, molalities, pH and saturation indices as a function of geological conditions i.e., 197.3 atm and 318.1 K. It allows the concentrations of element to be adjusted to measure equilibrium (or a gas partial pressure or specified saturation index) with a specific phase. The saturation index (SI) for the mineral can be defined in equation 2.

$$SI_p = log \prod_m^{M_{aq}} a_m^{Cm,p} \qquad 2$$

Equation 3 presents function used the equilibrium of the mineral as follows,

$$F_p = (ln\, K_p + [ln\ (10)]\ SI_p, target) - \sum_m^{M_{aq}} cm, pln(a_m) \qquad 3$$

Where $SI_p, target$ =target saturation index of mineral phase., *ln(10)* changes base *10 log* to natural *log.* The target SI would be specified. Zero, positive, or negative values specify equilibrium, supersaturation, and under saturation for the mineral in the solution. Moreover, $SI_p, target \cong$ log(partial pressure of the phase) for the fixed partial pressure of gas phase. Hence, the derivative of equation 4 relative to master unknown is,

$$dF_p = -\sum_m^{M_{aq}} cm, p\ dlna_m \qquad 4$$

We run simulation and determine that the saturation index SI of both salts in the presence of NH_3 and water. Firstly, if SI<0 the minerals could dissolve. Secondly, precipitates of minerals could occur if SI>0 (Parkhurst and Appelo, 2013). Thirdly, if SI~0, the minerals could either dissolve or precipitate to maintain the equilibrium (Charlton and Parkhurst, 2011). Figure 4b and c shows that the dissolution of each salt i.e., halite and anhydrite reduce after addition of NH_3 in the water when compared to pure water. These findings indicate that NH_3 minimizes the dissolution behavior of halite and anhydrite and might have not influenced the stability of

the cavern. Figure 4d shows that we have compared our findings with reference works to measure the solubility of NH_3 in water at geological conditions i.e., 197.3 atm and 45 °C. Further, results show halite and anhydrite do not react and precipitate in the NH_3 water solution and these rocks have potential to store NH_3 without mineralogical alteration and contamination issues. However, some portion of NH_4^+ would remain in the water and could influence the dissolution behavior of rocks. Hence, we observe that very minute concentrations of NH_4^+ could dissolve in the Halite+Water and Anhydrite+Water systems. However, this concentration could slightly increase with higher concentrations of NH_3 in the salt solutions (Figure 4 e and f). Thus, these ions are holding positive charge and ionizable (strong) (Scherer, 1993) when compared to NH_3 which is non-ionizable (weak) (Gonçalves et al., 1999) and therefore it could influence hydrogeochemistry and minerology of salt cavern. Typically, salt caverns can contain halite and anhydrite salts. Thus, it is noteworthy to determine the release of NH_4^+ and their effect on the phase stability of halite, anhydrite, and water systems. Consequently, high dissolution and precipitations problems can minimize the geological integrity of salt cavern and develop contamination issues which may affect NH_3 salt cavern geological storage security.

Storage of H_2 and NH_3 in depleted gas reservoirs can develop precipitation and dissolution of minerals. Hemme et al found that k-feldspar, dolomite and kaolinite precipitate in the reservoir rock in the presence of H_2 at 40 atm and 40 °C (Figure 5a). Similarly, we have used the one dimensional reactive mass transport (1DRMT) model using Phreeqc reported in (Hemme and Van Berk, 2018) and simulated change in the volume of mineral phases for H_2 and NH_3 (Figure 5a). We found that the values for change in the volume in the presence of H_2 match with previous study (Hemme and Van Berk, 2018). These findings show that quartz, calcite and illite dissolve after 30 years. Moreover, goethite, anhydrite, and barite completely dissolve in the H_2/brine water system during 30 years of the storage in the depleted gas reservoir. The

dissolution of goethite (FeO_2H) mineral augments the effect of H_2S production in the geological formation which contains sulphates and sulphides. Hence, the amount of Fe(+II) reduces from Fe (+III) and reacts with aqueous sulfide and generates pyrite (FeS_2) hence the sulfide is no more available for the generation of H_2S (Hemme & Van Berk, 2018). Small quantity of calcite precipitates due to dissolution of anhydrite leading to formation of aqueous Ca^{2+} in the reservoir (Figure 5a). Precipitation is opposite process of dissolution where ions come together and form solid minerals. The mechanism of precipitation is dependent on variety of factors including pressure, temperature, and pH of solution. In our case, all the minerals react with NH_3 and NH_4^+OH and precipitate in the reservoir rock. However, quartz dissolves in the NH_4^+OH and show no precipitation. Compounds consist of anions i.e., hydroxide (OH^-), sulfide (S^{2-}), and phosphate (PO_4^{3-}) are often not soluble in water (Figure 5a). These anions can form precipitates or solid deposits in the presence of cation ions i.e., Fe^{2+}, and Ca^{2+} etc., Consequently, precipitates of goethite (FeO_2H), pyrite (FeS_2), and calcite ($CaCO_3$) were formed after its reaction with NH_4OH. Moreover, the system yields large amount of precipitates of kalifeldspar, illite, and kaolinite clays precipitates after NH_3 its reacts with reservoir rock (Figure 5a). This might be possible that the clays have adsorbed large quantity of NH_4OH due to its large adsorption and cation ion exchange capacities leading to high quantity of OH- and its reactions with cations in the clays.

Achieving ammonia Geological Security

H_2 compresses at 691-789 atm to meet the vehicle tank storage requirements, which results in an energy consumption of 0.1 MJ/MJ. This figure is slightly higher at 0.29 MJ/MJ over 200 Km. Research reports estimate higher energy losses during H_2 liquification and transportation than NH_3 (Koike et al., 2012; Valera-Medina et al., 2018). Figure S4 illustrates that NH_3 has a high energy storage capacity when compared to H_2 in pipelines, storage tanks and salt caverns. Underground caverns are an environmentally friendly, cost effective and safe method for H_2

energy storage, yet have not been used for NH_3 storage (Aftab et al., 2022; Hassanpouryouzband et al., 2021). Figure 6 shows sustainable NH_3 production, geological storage opportunities and operational challenges.

Abandoned mines, hard rock, and salt caverns are potential NH_3 geological storage sites. However, a potential challenge is that NH_3 could dissolve into the formation water and may present additional difficulties during withdrawal and lead to NH_3 loss. By contrast, H_2 does not readily dissolve in depleted gas reservoirs, may not achieve solubility trapping, and could increase leakage risks (Hashemi et al., 2021; Ramesh Kumar et al., 2021).

Both NH_3 and NH_4^+OH ions could react with geological formations and may influence the pore-network system at the quantum scale (Day and Huitt, 1967). A wide range of NH_3 salts including ammonium lauric, and poly-quaternary ammonium contain clay swelling inhibition properties (Gholami et al., 2018). Thus, a reduction in clay swelling augments the permeability of the rock, minimizes pore-scale instabilities and has positive implications on NH_3 withdrawal from the reservoir (Figure S5).

Reservoir pressure support is critical to any successful implementation of NH_3 storage because NH_3 or NH_4^+OH water solutions require high reservoir pressure for withdrawal when compared to H_2 due to the difference in the density. Like H_2, NH_3 injection/production cycles in depleted reservoirs could influence the fracture pressure, hysteresis wettability effects, rock fatigue, and withdrawal efficiency parameters. NH_3 has a low diffusivity in water in comparison to H_2 when calculated using the Modified Stokes-Einstein and Wilke-Chang equations (Ferrell and Himmelblau, 1967; Frank et al., 1996). We predict concentrations of aqueous species i.e., OH^-, HCO_3^-, CH_4, $Al(OH)_4^-$, $CaHCO_3^+$, $CaOH^+$, $MgHCO_3^+$, H_4SiO_4, $H_3SiO_4^-$,$MgOH^+$, H_2S, HS^-. H_2, NH_4^+ and NH_3 do not considerably change after reacting with H_2 and results are same as reported in the study (Hemme and Van Berk, 2018). However, NH_3 is reactive with the above

aqueous species (Figure 5b). We examine the transport of non-reactive H_2 and reactive NH_3 from reservoir rock to cap rock through the simulation. This would help us to evaluate the geological storage security of the fluids. PHREEQC can model various 1D transport processes i.e., diffusion, advection, advection and dispersion with diffusion in the dual porosity zones.

The change of mass of a chemical transport through the reservoir rock is given by following advection-reaction-dispersion equation 5.

$$\frac{\partial \mathrm{C}}{\partial \mathrm{t}} = -\mathrm{V}\frac{\partial \mathrm{C}}{\partial \mathrm{x}} + D_L \frac{\partial^2 \mathrm{C}}{\partial^2 \mathrm{t}} - \frac{\partial q}{\partial t} \qquad 5$$

Where C is concentration of stored gas (i.e., H_2 or NH_3) in mol/kgw, t is modeled time (i.e., 0-30 years and 0-300 years), v is flow velocity of stored gas (m/s), x distance in meter, D_L is hydrodynamic dispersion coefficient (m^2/s).

$$D_L = D_e + \propto_L v \qquad 6$$

Where D_e is the effective diffusion coefficient, $\propto_L$ is the dispersivity in m, q is concentration in the solid phase (mol/kgw in the pores). $-\mathrm{V}\frac{\partial \mathrm{C}}{\partial \mathrm{x}}$ is the term for advective transport, $D_L \frac{\partial^2 \mathrm{C}}{\partial^2 \mathrm{t}}$ is dispersive transport, and $\frac{\partial q}{\partial t}$ is the change in the concentration in the solid due to reactions. Note that q and C have same unit and v and D_L are equal for all solute species. C is the total dissolved concentration for an element, including all redox species. We use default Cauchy/flux-flux/third type boundary condition in PHREEQC as provided in equation 7 ,

$$C(x_{end}, t) = C_o + \frac{D_L}{\mathrm{v}} \frac{\partial C(x_{end}, t)}{\partial x} \qquad 7$$

C_o is the displacing solution concentration and x_{end} is end of boundary. Note that both first and last boundaries are default closed or flux-flux.

We take H_2 gas, consider cap-rock porosity of 5%, and assume no fault system and conduct simulation through the rock. Figure S6 a and b and shows that a non-reactive H_2 (more than 4.0×10^{-7} molkgw^{-1} with diffusion coefficient of 5.13×10^{-9} m^2 s^{-1} moves up from reservoir

rock to cap rock and covers the distance of less than 4 m over 30 years (Hemme and Van Berk, 2018). We have adopted the same methodology as discussed in the (Hemme and Van Berk, 2018) and measured the presence of H_2 through the reservoir and found that our findings (Figure S6 c to d) well match with previous study (Hemme and Van Berk, 2018). Overall, storage of H_2 can be only seen in the first few meters of sealing rock. Besides each aqueous species migrate with a different rate of diffusion, generally the migration process of H_2 is very small and does not reveal any noticeable deviation over the modeled time of 30 years in the model. For longer storage times, the dissolved H_2 has more time to diffuse into sealing rock. After 300 years, H_2 diffuses 10 m via sealing rock. We have determined migration of NH_3 which (with diffusion coefficient 2.2×10^{-11}) from reservoir rock to sealing rock and found that H_2 significantly migrates upward (Figure S6 c and d) when compared to NH_3 (Figure 5 c and d). Hence, we have found that NH_3 moves up to sealing rock for first few meters (184 to 182 cell) with an amount of 2.0×10^{-7} mol kgw^{-1} over the modeled period of 30 years (Figure 5c). Moreover, we have observed that less than 1.0×10^{-7} mol kgw^{-1} amount of NH_3 diffuses 4 m into sealing rock over the modeled time of 300 years in the model (Figure 5d). Hence, sealing rock facilitates long term storage security for both fluids and does not leakage problems. However, minerals of reservoir rock react with NH_3 and precipitate which result in contamination insecurity leading to inappropriate NH_3 injection-withdrawing-reinjection issues. Figure S7 illustrates liquid NH_3 storage in a typical salt cavern under 40 °C and 197.3 atm pressure conditions.

Key points

This work constitutes significant research to achieve a Net-Zero target via H_2 chemical energy carrier i.e., NH_3. We conduct this research, develop NH_3 geo storage thought and demonstrate the facts for field scale deployment of NH_3 geo storage to make a critical difference in the present global energy scenario.

i. We confirm ζ_{NH_3} is significantly high when compared to ζ_{H_2}. It means more NH_3 can store at low pressures and temperatures than H_2 at geo storage conditions. Thus, H_2 storage will need high pressures and low temperature conditions making its surface storage difficult and energy intensive. NH_3 can transform into liquid at geo storage conditions. NH_3 carries the chemical H_2 and can liquify while shipping to transport the H_2 energy through a less energy intensive process.

ii. H_2 can quickly move to bigger pores, escape from the pore-network system, and leak via fault and seepage lines due to the low viscosity. However, NH_3 will not freely move in the porous reservoir rock incurring fewer chances of leakage. However, NH_3 storage deems practically difficult in a depleted reservoir.

iii. We measure the solubility of H_2 is very low compared to NH_3. This shows H_2 will hardly achieve solubility trapping in the rock. The chances of capillary and residual trapping are high for H_2 geo storage in brine saturated reservoir rock due to its high water-wet at geo storage conditions. However, NH_3 mixes in water and dissociates into NH_4^+ and NH_4^+OH. Through surface tension property of NH_3 in water, we noticed that the interfacial tension of NH_3/water solution decreases with the increasing concentration of NH_3 due to low cohesive forces within each liquid are weaker. Typically, low interfacial energy can increase the wettability of NH_3/water on the rock surface which could impact the geological storage security.

iv. Halite and anhydrite increase the pH of NH_3/water. The high alkalinity of the solution could establish a reaction with reservoir rock consequently reduce NH_3 injection and withdrawing cycle due to contamination of pore network system. For NH_3 geo storage in salt cavern, we measure the SI of NH_3/Salts/Water. For example, salts are halite and anhydrite, which are major components of uniform and interbedded salt domes. Our findings reveal that neither halite nor anhydrite can develop the problem of precipitation

in the cavern at geo storage conditions. Consequently, NH_3 can be stored in the salt cavern with minimum risk of contamination issues.

v. We conduct a simulation and determine the hydrogeochemical effect of NH_3/water solution on the variety of the minerals in depleted gas reservoir. Our findings reveal NH_3 is more reactive on calcite and illite compared to H_2. Moreover, quartz changes from supersaturated to slightly saturated conditions after reacting with NH_3. However, quartz remains supersaturated after reacting with H_2. These findings display risk of mineralogical changes in the reservoir rock after reacting with NH_3.

vi. We assume storage of H_2 and NH_3 in fault free reservoir rock. We found that less volume of NH_3 can migrate up from the underlying reservoir rock to caprock when compared to H_2. Generally, NH_3 and H_2 show very little change in the volume through reservoir to caprock in the modeled period implying the geological storage security.

vii. Lastly, NH_3 can rise environmental problems if it would leak at surface. It is toxic when compared to H_2. However, explosive safety of NH_3 is high when compared to H_2 in air due to its low upper-lower flammability limits. Consequently, the surface storage of H_2 has limitations of high explosive risk and requires large volume storage vessels/tank/pipeline than NH_3.

Clearly, there is much to be done. Each geological site presents unique issues that require further investigation. Critical unresolved issues that relate to depleted gas reservoirs include NH_3 solubility and diffusivity in formation water, interfacial tension between the formation water and NH_3, and rock-brine-NH_3 wettability at in-situ reservoir conditions. Therefore, salt cavern remains an essential choice for NH_3 storage. However, hydrogeochemical changes in the interbedded formations including carbonate and mudstone could be a challenge. Finally, resolution of these challenges will help us to achieve grid-scale storage and utilization of NH_3 for a clean and sustainable energy system.

Acknowledgement

First, the author would like to acknowledge the support of the RTP PhD Scholarship T2 2021 at Curtin University, Australia, and the visiting researcher opportunity at King Abdullah University of Science and Technology, Saudi Arabia.

References

Airgas, 2016. Aqua ammonia - Airgas Specialty Products. http://airgasspecialtyproducts.com/wp-content/uploads/2016/02/Physical_Properties-1.pdf. Assessed on 16th April 2022.

Aftab, A., Hassanpouryouzband, A., Xie, Q., Machuca, L.L. and Sarmadivaleh, M., 2022. Toward a Fundamental Understanding of Geological Hydrogen Storage. Industrial & Engineering Chemistry Research, 61(9): 3233-3253.

Aftab, A., Hassanpouryouzband, A., Martin, A., Kendrick, J. E., Thaysen, E. M., Heinemann, N., ... & Edlmann, K. (2023). Geochemical integrity of wellbore cements during geological hydrogen storage. Environmental science & technology letters, 10(7), 551-556.

Alemu, B.L., Aker, E., Soldal, M., Johnsen, Ø. and Aagaard, P., 2013. Effect of sub-core scale heterogeneities on acoustic and electrical properties of a reservoir rock: a CO_2 flooding experiment of brine saturated sandstone in a computed tomography scanner. Geophysical Prospecting, 61(1): 235-250.

Alejandre, J., Tildesley, D.J. and Chapela, G.A., 1995. Molecular dynamics simulation of the orthobaric densities and surface tension of water. The Journal of chemical physics, 102(11): 4574-4583.

Ali, A. M., Padmanabhan, E., Mijinyawa, A., & Kwaya, M. Y. (2019). Effect of pH on the stability of quartz in a multi-phase system of kaolinite, hydrous Al (hydr)oxide and quartz. SN Applied Sciences, 1(5), 1-11.

Alshameri, A., He, H., Zhu, J., Xi, Y., Zhu, R., Ma, L. and Tao, Q., 2018. Adsorption of ammonium by different natural clay minerals: characterization, kinetics and adsorption isotherms. Applied Clay Science, 159: 83-93.

Andersson, J. and Grönkvist, S., 2019. Large-scale storage of hydrogen. International journal of hydrogen energy, 44(23): 11901-11919.

Arnold, J.H., 1930. Studies in diffusion. II. A kinetic theory of diffusion in liquid systems. Journal of the American Chemical Society, 52(10): 3937-3955.

Ballinger, T., Overland, J., Wang, M., Bhatt, U., Hanna, E., Hanssen-Bauer, I., Kim, S.-J., Thoman, R. and Walsh, J., 2020. Arctic report card 2020: Surface air temperature.

Berdyanskaya, R. A., Golyand, S. M., & Chertkov, B. A. (1959). On the partial pressure of SO_2 over ammonium sulfite-bisulfite solutions. Zh. Prikl. Khim, 37, 1930-1936.

Bertie, J.E. and Shehata, M.R., 1984. Ammonia dihydrate: Preparation, x-ray powder diffraction pattern and infrared spectrum of $NH_3{\cdot}2H_2O$ at 100 K. The Journal of chemical physics, 81(1): 27-30.

Bremner, J. and Tabatabai, M., 1972. Use of an ammonia electrode for determination of ammonium in Kjeldahl analysis of soils. Communications in Soil Science and Plant Analysis, 3(2): 159-

165.Caglayan, D.G., Weber, N., Heinrichs, H.U., Linßen, J., Robinius, M., Kukla, P.A. and Stolten, D., 2020. Technical potential of salt caverns for hydrogen storage in Europe. International Journal of Hydrogen Energy, 45(11): 6793-6805.

Carlson, T., 1911. The diffusion of oxygen in water. Journal of the American Chemical Society, 33(7): 1027-1032.

Celik, S., 2020. The effects of climate change on human behaviors, Environment, climate, plant and vegetation growth. Springer, pp. 577-589.

Cesaro, Z., Ives, M., Nayak-Luke, R., Mason, M. and Bañares-Alcántara, R., 2021. Ammonia to power: Forecasting the levelized cost of electricity from green ammonia in large-scale power plants. Applied Energy, 282: 116009.

Council, N.R. and Levels, C.o.A.E.G., 2008. Ammonia Acute Exposure Guideline Levels, Acute Exposure Guideline Levels for Selected Airborne Chemicals: Volume 6. National Academies Press (US).

Charlton, S.R. and Parkhurst, D.L., 2011. Modules based on the geochemical model PHREEQC for use in scripting and programming languages. Computers & Geosciences, 37(10): 1653-1663.

Chattot, R.l., 2017. Surface Distortion and Electrocatalysis: Structure-Activity Relationships for the Oxygen Reduction Reaction on PtNi/C Nanocatalysts, Université Grenoble Alpes.

Chen, C., Guerit, L., Foreman, B.Z., Hassenruck-Gudipati, H.J., Adatte, T., Honegger, L., Perret, M., Sluijs, A. and Castelltort, S., 2018. Estimating regional flood discharge during Palaeocene-Eocene global warming. Scientific Reports, 8(1): 1-8.

Clifford, I. and Hunter, E., 2002. The System Ammonia–Water at Temperatures up to 150 °C. and at Pressures up to Twenty Atmospheres. The Journal of Physical Chemistry, 37(1): 101-118.

Davidson, J., 1957. The determination of diffusion coefficient for sparingly soluble gases in liquids. Trans. Instn Chem. Engrs., 35: 51-60.

Day, J.J. and Huitt, J., 1967. Laboratory study of rock softening and means of prevention during steam or hot water injection. Journal of Petroleum Technology, 19(05): 703-711.

Ding, M. H., Wang, X., Bian, L. G., Jiang, Z. N., Lin, X., Qu, Z. F., & Zhu, K. J. (2024). State of polar climate in 2023. Advances in Climate Change Research.

EIA, 2019. Global CO_2 emissions in 2019, https://www.iea.org/articles/global-CO_2-emissions-in-2019?__cf_chl_captcha_tk__=pmd_c5b276517e0d0267169834165e9b8ebed88f5170-1627309483-0-gqNtZGzNAuKjcnBszQiO. Accessed on 26th July 2021.

Energy, 2021. Hydrogen Storage - Basics, https://www.energy.gov/eere/fuelcells/hydrogen-storage-basics-0. Accessed on 26th July 2021.

EngineeringTool, 2022. Explosive concentration limits. https://www.engineeringtoolbox.com/explosive-concentration-limits-d_423.html. Assesed on 11th June.

Erickson, R.J., 1985. An evaluation of mathematical models for the effects of pH and temperature on ammonia toxicity to aquatic organisms. Water Research, 19(8): 1047-1058.

Eric W. Lemmon, I.H.B., Marcia L. Huber, and Mark O. McLinden, 2022. "Thermophysical Properties of Fluid Systems" in NIST Chemistry WebBook, NIST Standard Reference Database Number 69 Eds. P.J. Linstrom and W.G. Mallard, National Institute of Standards and Technology, Gaithersburg MD, 20899, https://doi.org/10.18434/T4D303, Assessed on 16th April.

Espinoza, D.N. and **Santamarina, J.C**., 2017. CO_2 breakthrough—Caprock sealing efficiency and integrity for carbon geological storage. International Journal of Greenhouse Gas Control, 66: 218-229.

EU, 2021. Paris Agreement, https://ec.europa.eu/clima/policies/international/negotiations/paris_en. Accessed on 26th July 2021.

Ferrell, R. and Himmelblau, D., 1967. Diffusion coefficients of hydrogen and helium in water. AIChE Journal, 13(4): 702-708.

Flammability, 2022. Gases - Explosion and Flammability Concentration Limits. https://www.engineeringtoolbox.com/explosive-concentration-limits-d_423.html. Assessed on April 16th 2022.

Frank, M.J., Kuipers, J.A. and van Swaaij, W.P., 1996. Diffusion coefficients and viscosities of CO_2+ H_2O, CO_2+ CH_3OH, NH_3+ H_2O, and NH^{3+} CH_3OH liquid mixtures. Journal of chemical & engineering data, 41(2): 297-302.

Franklin, E. and Kraus, C., 1899. Some properties of liquid ammonia. Chem. J, 21: 8-14.

Franklin, E. C. (1935). Heterocyclic Nitrogen Compounds. I. Pentacyclic Compounds. Chemical Reviews, 16(3), 305-361.

Gummer, J. and Hawksworth, S.J., 2008. Spontaneous ignition of hydrogen-Literature review. Accessed on Jan 1st 2024.

Gao, K., Wu, J., Bell, I. and Lemmon, E., 2019. Thermodynamic properties of ammonia for temperatures from the melting line to 725 K and pressures to 1000 MPa. J. Phys. Chem. Ref. Data (to be submitted).

Gholami, R., Elochukwu, H., Fakhari, N. and Sarmadivaleh, M., 2018. A review on borehole instability in active shale formations: Interactions, mechanisms and inhibitors. Earth-Science Reviews, 177: 2-13.

Gonçalves, A.-M., Mathieu, C., Herlem, M. and Etcheberry, A., 1999. Oxygen reduction mechanisms at p-InP and p-GaAs electrodes in liquid ammonia in neutral buffered medium and acidic media. Journal of Electroanalytical Chemistry, 462(1): 88-96.

Gravities, S., 2022. Gases - Specific Gravities Specific gravities of air, ammonia, butadiene, carbon dioxide, carbon monoxide and some other common gases. https://www.engineeringtoolbox.com/specific-gravities-gases-d_334.html. Assessed on 16th April 2022.Green, D.W. and Perry, R.H., 2008. Perry's chemical engineers' handbook. McGraw-Hill Education.

Grilly, E., 1951. The Vapor Pressures of Hydrogen, Deuterium and Tritium up to Three Atmospheres1. Journal of the American Chemical Society, 73(2): 843-846.

Hadjipanayiotou, M., Verhaeghe, L., Goodchild, T. and Shaker, B., 1993. Ammoniation of straw using urea, ammonia gas or ammonium hydroxide. Livestock Research for Rural Development, 5(3).

Halseid, R., Vie, P.J. and Tunold, R., 2006. Effect of ammonia on the performance of polymer electrolyte membrane fuel cells. Journal of Power Sources, 154(2): 343-350.

Hashemi, L., Blunt, M. and Hajibeygi, H., 2021. Pore-scale modelling and sensitivity analyses of hydrogen-brine multiphase flow in geological porous media. Scientific reports, 11(1): 1-13.

Hassanpouryouzband, A., Farahani, M.V., Yang, J., Tohidi, B., Chuvilin, E., Istomin, V. and Bukhanov, B., 2019. Solubility of flue gas or carbon dioxide-nitrogen gas mixtures in water and aqueous solutions of salts: Experimental measurement and thermodynamic modeling. Industrial & Engineering Chemistry Research, 58(8): 3377-3394.

Hassanpouryouzband, A., Joonaki, E., Edlmann, K. and Haszeldine, R.S., 2021. Offshore Geological Storage of Hydrogen: Is This Our Best Option to Achieve Net-Zero? ACS Energy Letters, 6: 2181-2186.

Hawkes, S.J., 2004. The formula for ammonia monohydrate. Journal of Chemical Education, 81(11): 1569.

Hemme, C. and Van Berk, W., 2018. Hydrogeochemical modeling to identify potential risks of underground hydrogen storage in depleted gas fields. Applied Sciences, 8(11): 2282.

Huang, Ju-Chang, and Chii Shang. "Air stripping." Advanced physicochemical treatment processes (2006): 47-79.

Huber, M.L., Perkins, R.A., Laesecke, A., Friend, D.G., Sengers, J.V., Assael, M.J., Metaxa, I.N., Vogel, E., Mareš, R. and Miyagawa, K., 2009. New international formulation for the viscosity of H_2O. Journal of Physical and Chemical Reference Data, 38(2): 101-125.

IEA, 2019. The Future of Hydrogen. https://www.iea.org/reports/the-future-of-hydrogen. Accessed on 12th July 2022.

IEA-AMP, 2022. Ammonia. https://www.iea-amf.org/content/fuel_information/ammonia. Assessed on 17th April 2022.

Iglauer, S., 2021. Optimum geological storage depths for structural H_2 geo-storage. Journal of Petroleum Science and Engineering: 109498.

INCHEM, 2022. Ammonia (Anhydrous). https://inchem.org/documents/icsc/icsc/eics0414.htm. Assses on 16th April 2022.

James, D. and Harward, M., 1962. Mechanism of NH_3 adsorption by montmorillonite and kaolinite. Clays and Clay Minerals, 11(1): 301-320.

Jackson, A., & Solbett, J. M. (1955). Sulphuric Acid Plant-Tail Gas Treatment. Chemistry & Industry, (42), 1304-1311.

Johnson, J., 2019. The pH of water: What to know. https://www.medicalnewstoday.com/articles/327185. Assessed on 15th April 2022.

Johnstone, H. F. (1935). Recovery of Sulfur Dioxide from Waste Gases Equilibrium Partial Vapor Pressures over Solutions of the Ammonia-Sulfur Dioxide-Water System. Industrial & Engineering Chemistry, 27(5), 587-593.

Kapeghian, J.C., Mincer, H.H., Jones, A.B., Verlangieri, A.J. and Waters, I.W., 1982. Acute inhalation toxicity of ammonia in mice. Bulletin of environmental contamination and toxicology, 29(3): 371-378.

Karabeyoglu, A. and Evans, B., 2012. Fuel conditioning system for ammonia fired power plants, NH_3 Congress, Iowa, USA.

Koike, M., Miyagawa, H., Suzuoki, T. and Ogasawara, K., 2012. Ammonia as a hydrogen energy carrier and its application to internal combustion engines. Sustainable vehicle technologies: driving the green agenda: 61-70.

Kojima, Y., 2014. Liquid ammonia for hydrogen storage. NH_3 Fuel Association. Referred, 20: 2017.

Kojima, Y. and Yamaguchi, M., 2021. Thermodynamic analysis of ammonia storage materials. International Journal of Hydrogen Energy, 46(21): 11756-11760.

Krishnan Rajeshwar, R.M. and Licht, S., 2008. Solar Hydrogen Generation Toward a Renewable Energy Future.

Laby, G.W.C.K.a.T.H., 1986. "Tables of Physical and Chemical Constants," 15th ed., Longman, NY, 1986, p. 219.

Laesecke, A. and Muzny, C.D., 2017. Reference correlation for the viscosity of carbon dioxide. Journal of physical and chemical reference data, 46(1): 013107.

Lagowski, J., 1978. The chemistry of liquid ammonia. Journal of Chemical Education, 55(12): 752.

Leachman, J.W., Jacobsen, R.T., Penoncello, S. and Lemmon, E.W., 2009. Fundamental equations of state for parahydrogen, normal hydrogen, and orthohydrogen. Journal of Physical and Chemical Reference Data, 38(3): 721-748.

Lemmon, E.W. and Jacobsen, R.T., 2004. Viscosity and thermal conductivity equations for nitrogen, oxygen, argon, and air. International journal of thermophysics, 25(1): 21-69.

Li, J., Dong, W., Oenema, O., Chen, T., Hu, C., Yuan, H. and Zhao, L., 2019. Irrigation reduces the negative effect of global warming on winter wheat yield and greenhouse gas intensity. Science of the Total Environment, 646: 290-299.

Li, K., Andersen, S.Z., Statt, M.J., Saccoccio, M., Bukas, V.J., Krempl, K., Sažinas, R., Pedersen, J.B., Shadravan, V. and Zhou, Y., 2021. Enhancement of lithium-mediated ammonia synthesis by addition of oxygen. Science, 374(6575): 1593-1597.

Lian, X., Piao, S., Chen, A., Huntingford, C., Fu, B., Li, L.Z., Huang, J., Sheffield, J., Berg, A.M. and Keenan, T.F., 2021. Multifaceted characteristics of dryland aridity changes in a warming world. Nature Reviews Earth & Environment, 2(4): 232-250.

Lindsey, R. and Dahlman, L., 2020. Climate change: Global temperature. Climate. gov, 16.

Liu, X., Kang, Y., Luo, P., You, L., Tang, Y. and Kong, L., 2015. Wettability modification by fluoride and its application in aqueous phase trapping damage removal in tight sandstone reservoirs. Journal of Petroleum Science and Engineering, 133: 201-207.

Mazloomi, K. and Gomes, C., 2012. Hydrogen as an energy carrier: Prospects and challenges. Renewable and Sustainable Energy Reviews, 16(5): 3024-3033.

Meys, R., Kätelhön, A., Bachmann, M., Winter, B., Zibunas, C., Suh, S. and Bardow, A., 2021. Achieving net-zero greenhouse gas emission plastics by a circular carbon economy. Science, 374(6563): 71-76.

Mogensen, M., Chen, M., Frandsen, H., Graves, C., Hansen, J., Hansen, K., Hauch, A., Jacobsen, T., Jensen, S. and Skafte, T., 2019. Reversible solid-oxide cells for clean and sustainable energy. Clean Energy, 3(3): 175-201.

Møller, K.T., Jensen, T.R., Akiba, E. and Li, H.-w., 2017. Hydrogen-A sustainable energy carrier. Progress in Natural Science: Materials International, 27(1): 34-40.

Monogenidou, S., Assael, M.J. and Huber, M.L., 2018. Reference Correlation for the Viscosity of Ammonia from the Triple Point to 725 K and up to 50 MPa. Journal of physical and chemical reference data, 47(2): 023102.

Moradi, H., Azizpour, H., Bahmanyar, H., Mohammadi, M. and Akbari, M., 2020. Prediction of methane diffusion coefficient in water using molecular dynamics simulation. Heliyon, 6(11): e05385.

Mørch, C.S., Bjerre, A., Gøttrup, M.P., Sorenson, S.C. and Schramm, J., 2011. Ammonia/hydrogen mixtures in an SI-engine: Engine performance and analysis of a proposed fuel system. fuel, 90(2): 854-864.

Muzny, C.D., Huber, M.L. and Kazakov, A.F., 2013. Correlation for the viscosity of normal hydrogen obtained from symbolic regression. Journal of Chemical & Engineering Data, 58(4): 969-979.

Nagaoka, K., Eboshi, T., Takeishi, Y., Tasaki, R., Honda, K., Imamura, K. and Sato, K., 2017. Carbon-free H_2 production from ammonia triggered at room temperature with an acidic $RuO_2/\gamma\text{-}A_{l2}O_3$ catalyst. Science advances, 3(4): e1602747.

NLM, 2022a. Ammonia. https://pubchem.ncbi.nlm.nih.gov/compound/Water. Assessed on 15th April 2022.

NLM, 2022b. Methane. https://www.ncbi.nlm.nih.gov/books/NBK208285/. Assessed on 15th April Perman, E.P., 1903. CXV.—Vapour pressure of aqueous ammonia solution. Part II. Journal of the Chemical Society, Transactions, 83: 1168-1184.

NASA, 2021. Overview: Weather, Global Warming and Climate Change, https://climate.nasa.gov/resources/global-warming-vs-climate-change/. Accessed on 26th July 2021.

NASA, 2022 Global Climate Change: Vital Signs of the Planet. https://climate.nasa.gov/. Accessed on 12th Feb 2022.

Ou, Y., Iyer, G., Clarke, L., Edmonds, J., Fawcett, A.A., Hultman, N., McFarland, J.R., Binsted, M., Cui, R. and Fyson, C., 2021. Can updated climate pledges limit warming well below 2°C? Science, 374(6568): 693-695.

Parkhurst, D.L. and Appelo, C., 2013. Description of input and examples for PHREEQC version 3—a computer program for speciation, batch-reaction, one-dimensional transport, and inverse geochemical calculations. US geological survey techniques and methods, 6(A43): 497.

Patel, A., Stamatakis, S., Young, S. and Friedheim, J., 2007. Advances in inhibitive water-based drilling fluids—can they replace oil-based muds?, International Symposium on Oilfield Chemistry. OnePetro.

Patonia, A. and Poudineh, R., 2020. Ammonia as a Storage Solution for Future Decarbonized Energy Systems. Oxford Institute for Energy Studies.

Paul, S. and Chandra, A., 2005. Liquid-vapor interfacial properties of water-ammonia mixtures: Dependence on ammonia concentration. The Journal of chemical physics, 123(17): 174712.

Perman, E.P., 1903. CXV.—Vapour pressure of aqueous ammonia solution. Part II. Journal of the Chemical Society, Transactions, 83: 1168-1184.

Popescu, M.-A., Isopescu, R., Matei, C., Fagarasan, G. and Plesu, V., 2014. Thermal decomposition of calcium carbonate polymorphs precipitated in the presence of ammonia and alkylamines. Advanced Powder Technology, 25(2): 500-507.

Price, J., Crofton, M. and Lee, Y.T., 1991. Vibrational spectroscopy of the ammoniated ammonium ions NH_4 (NH_3) n (n= 1-10). The Journal of Physical Chemistry, 95(6): 2182-2195.

Robinson, C. and Smith, D., 1984. The auto-ignition temperature of methane. Journal of hazardous materials, 8(3): 199-203.

Rajasegar, R., Mitsingas, C.M., Mayhew, E.K., Liu, Q., Lee, T. and Yoo, J., 2018. Development and characterization of additive-manufactured mesoscale combustor array. J. Energy Eng, 144(3): 04018013.

Ramesh Kumar, K., Makhmutov, A., Spiers, C.J. and Hajibeygi, H., 2021. Geomechanical simulation of energy storage in salt formations. Scientific Reports, 11(1): 1-24.

Rowlinson, J.S. and Widom, B., 2013. Molecular theory of capillarity. Courier Corporation.

Sanger, M.J. and Danner, M., 2010. Aqueous ammonia or ammonium hydroxide? Identifying a base as strong or weak. Journal of chemical education, 87(11): 1213-1216.

Santamarina, J.C., **Aftab, A.**, Espinoza, D.N., Dusseault, M., Gens, A., Hoteit, H., Kim, S., Lee, J., Lei, L., Narsilio, G., Pereira, J., Sanchez, M., Soga, K., Villar, M. and Violay, M., 2022. Energy geo-engineering, State of the Art Report, Proceedings of the 20th International Conference on Soil Mechanics and Geotechnical Engineering, Sydney, Australia.

Scherer, H., 1993. Dynamics and availability of the non-exchangeable NH_4-N—a review. European Journal of Agronomy, 2(3): 149-160.

Sedov, N.V. (1957). Nauch. Tekh. Inform. Byull. Nauch. Inst. po Udobren. i Insektofungisidam, 5–6 , pp. 79-104.

Speight, J.G., 2017. Lange's Handbook of Chemistry. McGraw-Hill Education, New York.

Sugahara, H., Takano, Y., Ogawa, N.O., Chikaraishi, Y. and Ohkouchi, N., 2017. Nitrogen isotopic fractionation in ammonia during adsorption on silicate surfaces. ACS Earth and Space Chemistry, 1(1): 24-29.

Szarawara J (1959). Studies on staties of the system: H_2O-NH_3-SO_2. II. Diphase equilibrium "solution-gas phase". Chem. Stosowana, 3, 395-425.

Thermophysical, 2022. Ammonia - Thermophysical Properties. https://www.engineeringtoolbox.com/ammonia-d_1413.html. Assessed on 16th April 2022.Tokarska, K.B. and Gillett, N.P., 2018. Cumulative carbon emissions budgets consistent with 1.5 °C global warming. Nature Climate Change, 8(4): 296-299.

UN, 2021. COP26: Together for our planet. UN. https://www.un.org/en/climatechange/cop26. Accessed on 24th April 2022.

USGS, 2019. pH and Water. https://www.usgs.gov/special-topics/water-science-school/science/ph-and-water#overview. Accessed on 17th April 2022.

Valera-Medina, A., Xiao, H., Owen-Jones, M., David, W.I. and Bowen, P., 2018. Ammonia for power. Progress in Energy and Combustion Science, 69: 63-102.

van Praagh, G. (1939). 'Acidity'of Quartz. Nature, 143(3634), 1068-1068.

Wagner, W. and Pruß, A., 2002. The IAPWS formulation 1995 for the thermodynamic properties of ordinary water substance for general and scientific use. Journal of physical and chemical reference data, 31(2): 387-535.

Wang, X., Chen, Q., Hu, H. and Yin, Z., 2011. Solubility and dissolution kinetics of quartz in NH_3–H_2O system at 25°C. Hydrometallurgy, 107(1-2): 22-28.

Ware, G.C., 1928. Surface tension of liquid ammonia and adsorption studies at its liquid vapor interface. Master of Science Thesis. Kansas State Agricultural College.

Warren, K.S., 1962. Ammonia toxicity and pH. Nature, 195(4836): 47-49.Warren, R., Price, J., Graham, E., Forstenhaeusler, N. and VanDerWal, J., 2018. The projected effect on insects, vertebrates, and plants of limiting global warming to 1.5 °C rather than 2 °C. Science, 360(6390): 791-795.

Waskom, M., 2014. Seaborn-Data. GitHub Repository. https://github.com/mwaskom/seaborn-data/blob/master/process/flights.py. Accessed on 19th March 2023.

Yoke, J.T., 1991. Ammonium Hydroxide: What is its structure? Journal of Chemical Education, 68(6): 533.

Yusaf, T., Laimon, M., Alrefae, W., Kadirgama, K., Dhahad, H.A., Ramasamy, D., Kamarulzaman, M.K. and Yousif, B., 2022. Hydrogen Energy Demand Growth Prediction and Assessment (2021–2050) Using a System Thinking and System Dynamics Approach. Applied Sciences, 12(2): 781.

Zhongming, Z., Linong, L., Xiaona, Y., Wangqiang, Z. and Wei, L., 2021. 2020 Tied for Warmest Year on Record, NASA Analysis Shows. https://www.nasa.gov/press-release/2021-tied-for-6th-warmest-year-in-continued-trend-nasa-analysis-shows. Accessed on 24th April 2020.

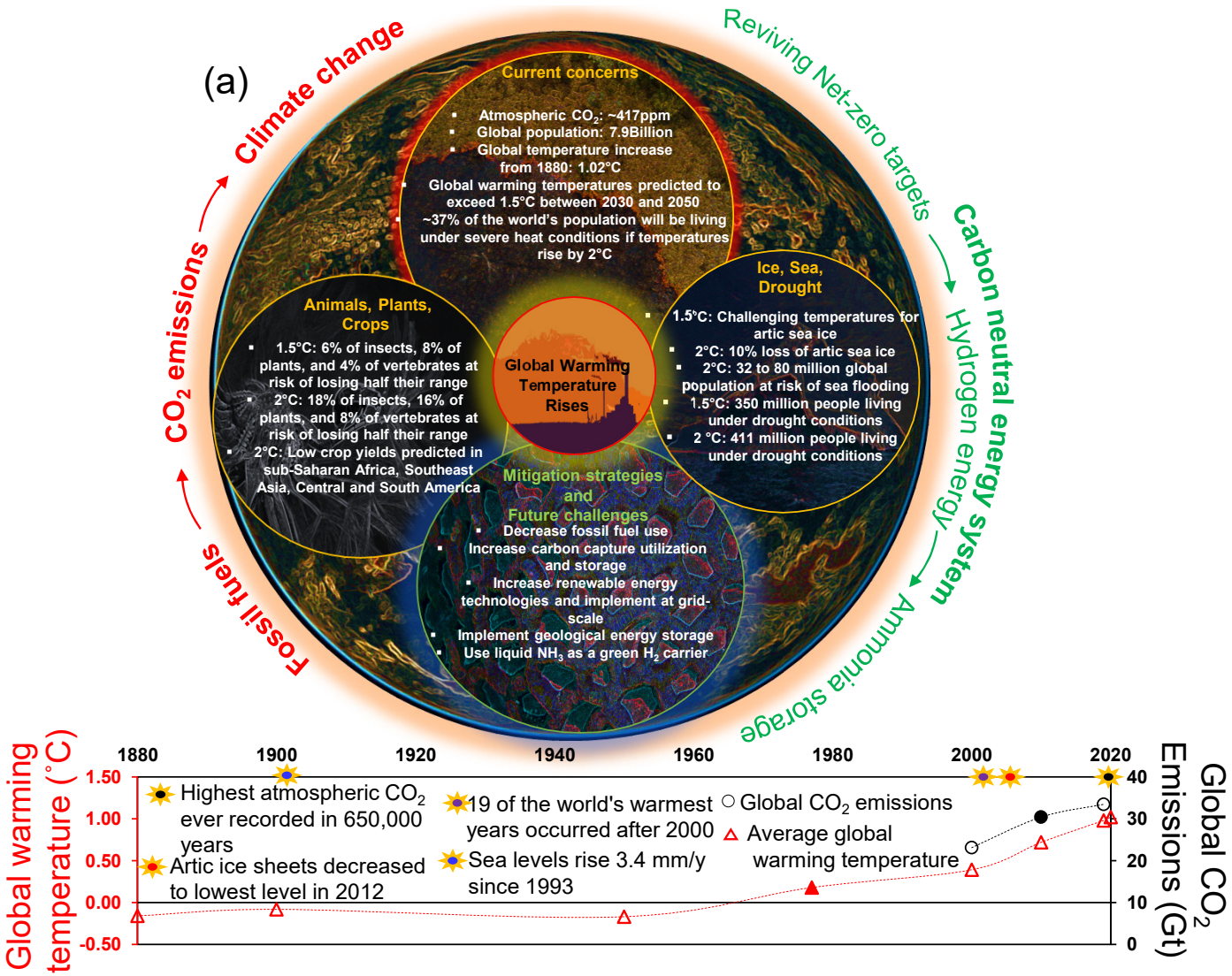

Figure 1 (a) Predicted impact of global warming and key challenges. The 10 warmest recorded events have occurred since 2005 and a further 0.5 °C increase in global average temperatures could trigger extreme heat waves, droughts and flooding events which will negatively impact ice sheets, sea levels, fauna, flora and associated crop yields. Data collected from (Lindsey and Dahlman, 2020;Ballinger et al., 2020; Zhongming et al., 2021;Lian et al., 2021;Li et al., 2019;Warren et al., 2018;NASA, 2022;Tokarska and Gillett, 2018;Chen et al., 2018;Celik, 2020).

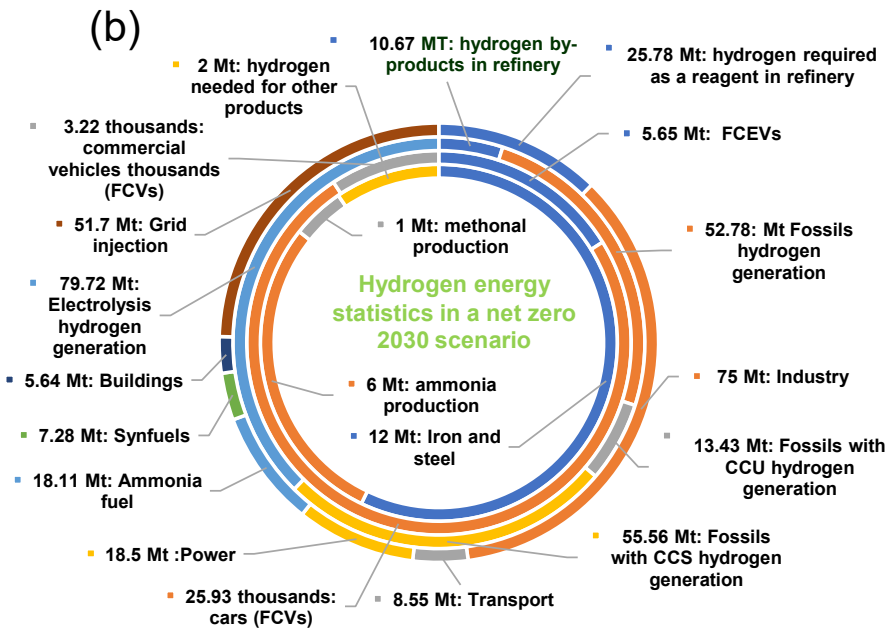

Figure 1 (b) Hydrogen energy statistics in a net zero 2030 scenario. Statistics show amounts of H_2 required for both industry, transport and civil and energy infrastructure (IEA, 2019).

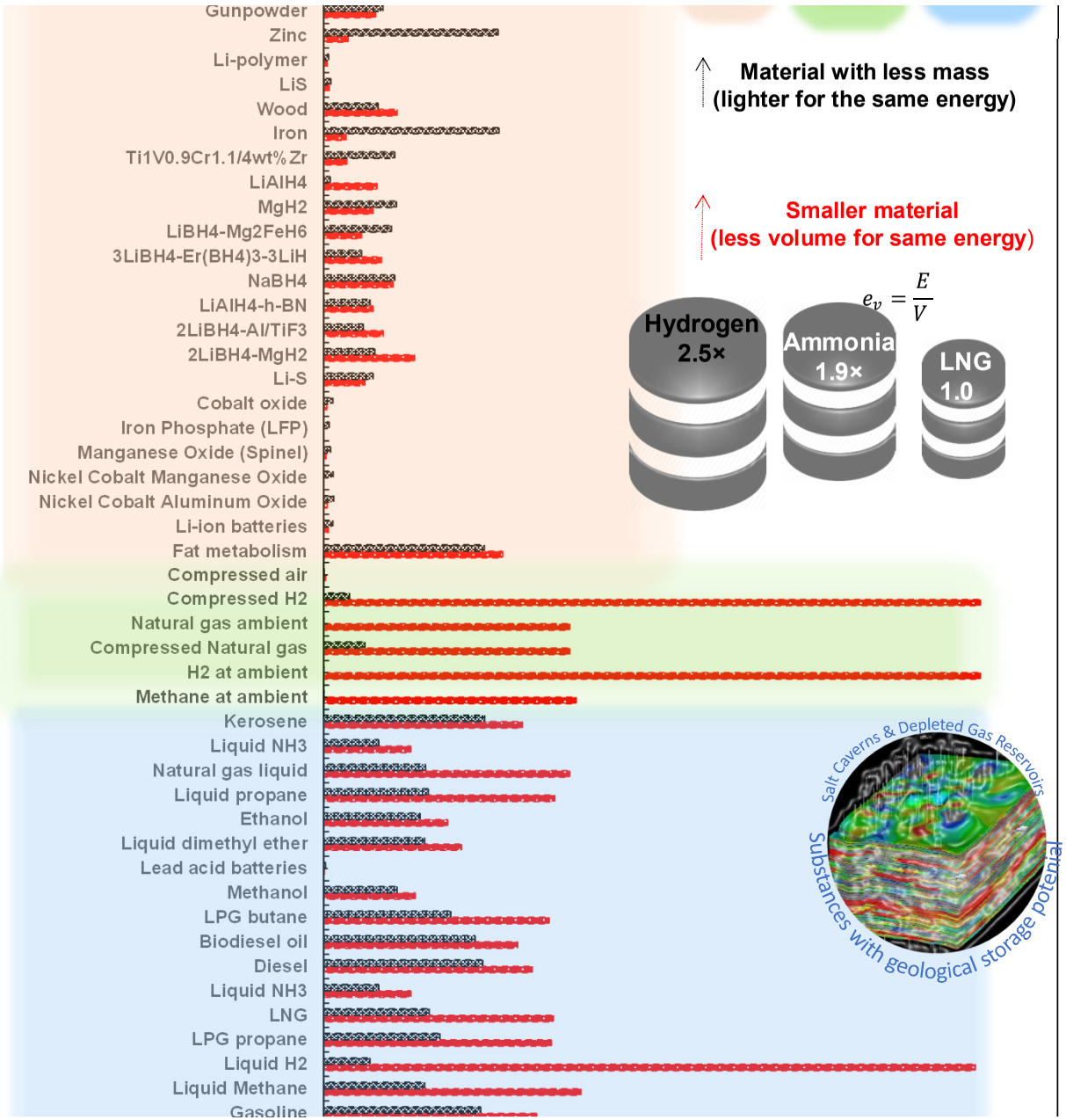

Figure 2 Gravimetric and volumetric energy density of various energy material. This figure shows that volumetric energy density of NH_3 is significantly in comparison to volumetric energy density of H_2 however inverse is true for gravimetric energy of H_2 in comparison to NH_3 (Mogensen et al., 2019; Mazloomi & Gomes, 2012; Sartbaeva et al., 2008).

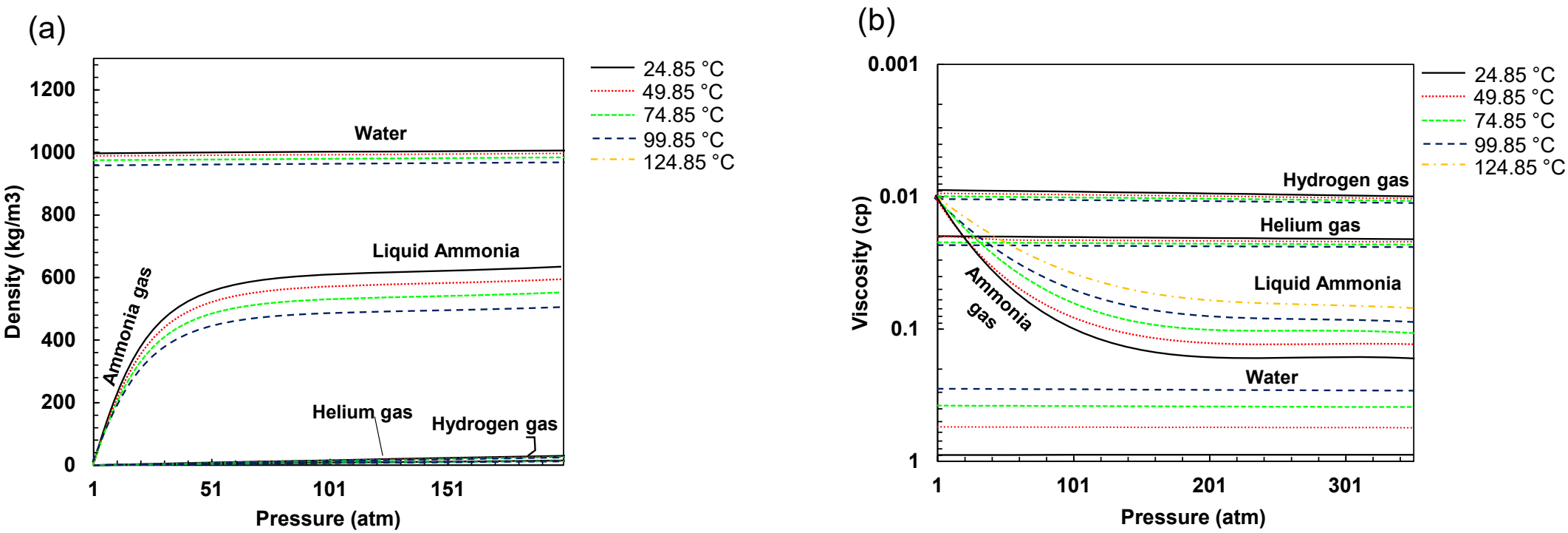

Figure 3 (a) Density of water, liquid NH_3, H_2 and He measured at variable temperature, and pressure (Gao et al., 2019; Leachman et al., 2009; Wagner and Pruß, 2002) (b) Results indicate that viscosity increases with pressure and remains stable at high pressure conditions (Huber et al., 2009; Monogenidou et al., 2018; Muzny et al., 2013).

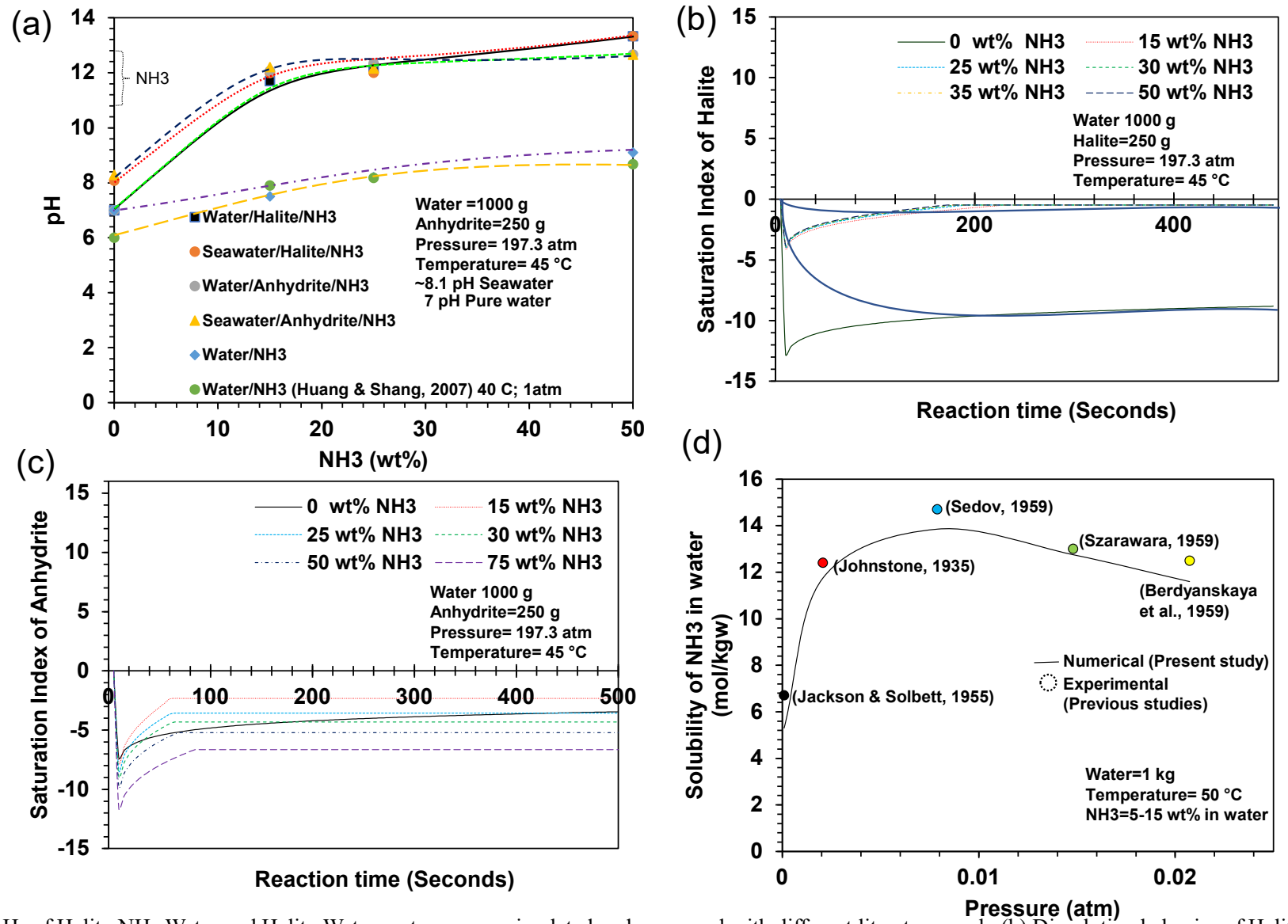

Figure 4 (a) pHs of Halite-NH_3-Water and Halite-Water systems were simulated and compared with different literature work. (b) Dissolution behavior of Halite in different concentrations of NH_3 (c) Dissolution behaviour of Anhydrite in different concentrations of NH_3 (d) Validation of our numerical study with previous reference works for solubility of NH_3 in water

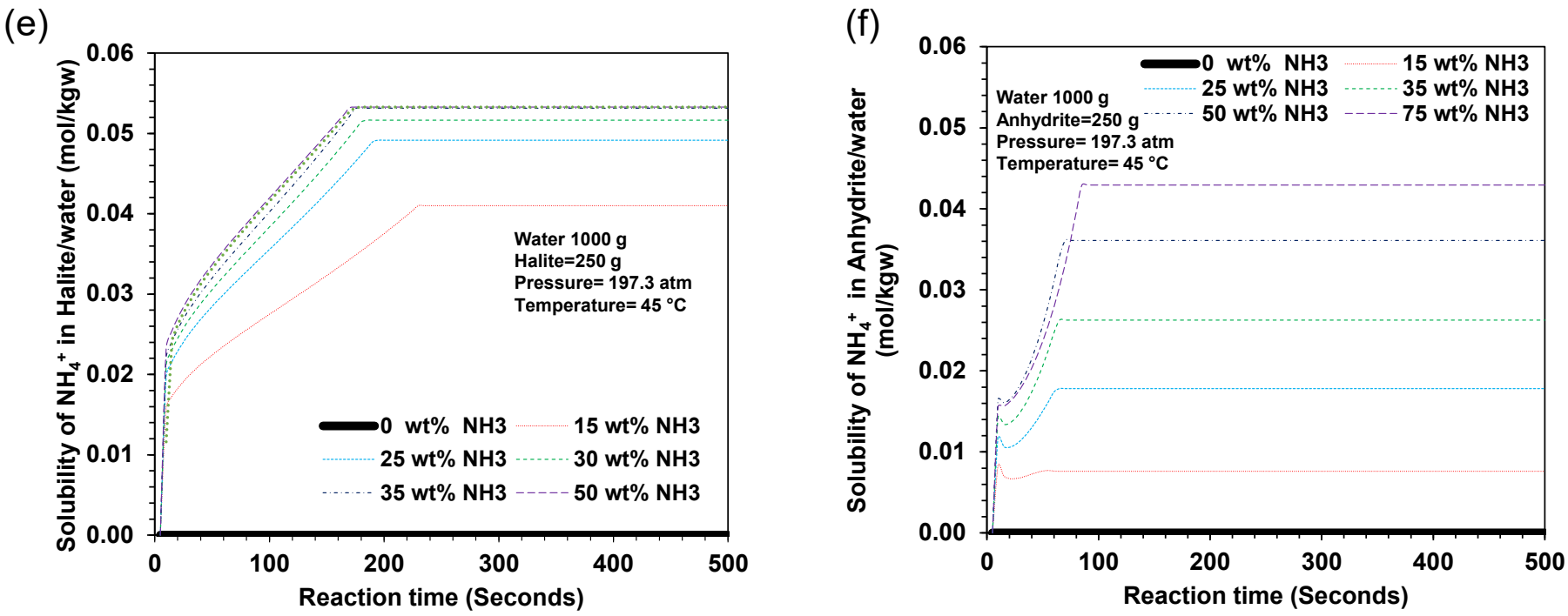

Figure 4 (e) Molarity of NH_4^+ in Halite/water solution (f) Molarity of NH_4^+ in Anhydrite/water solution.

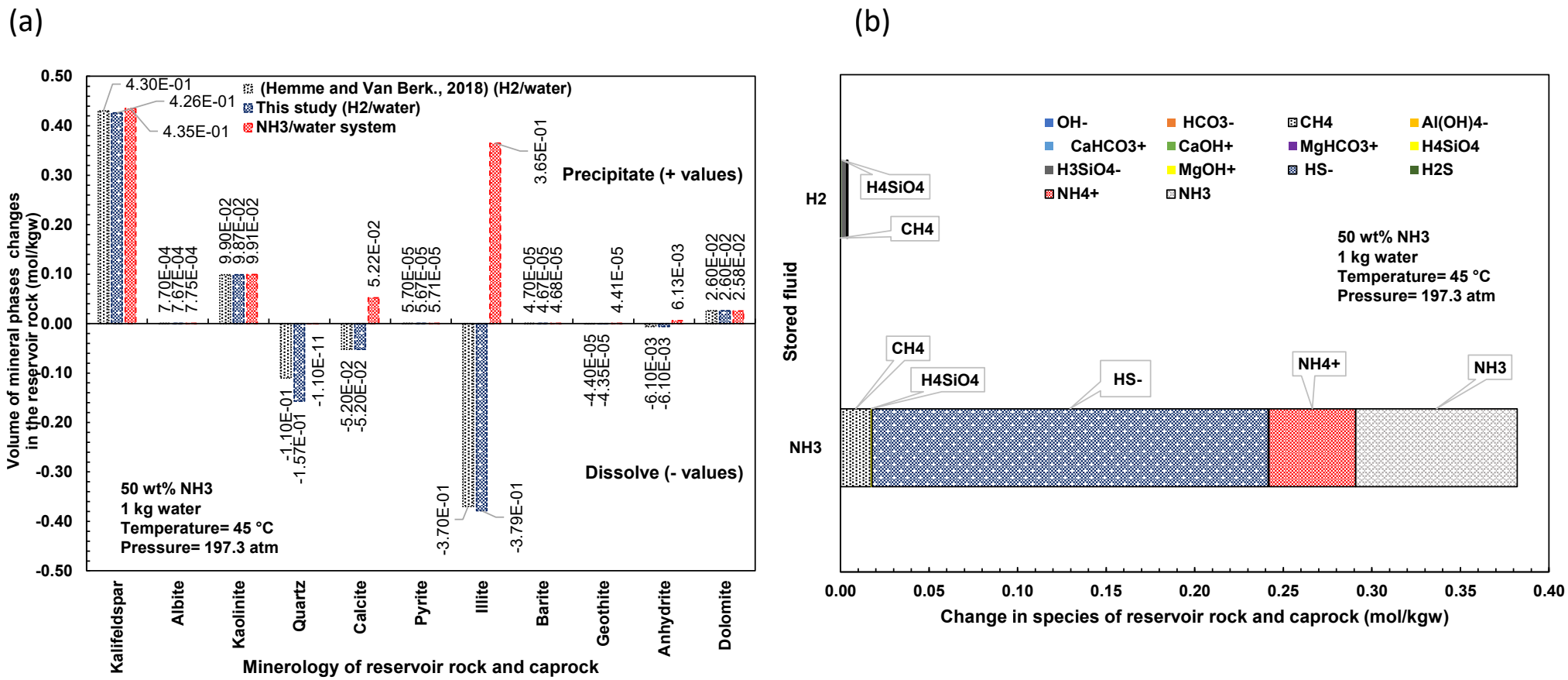

Figure 5 (a) Change in the volume of different minerals phases in the reservoir rock after 30 years in the presence of H_2 and NH_3 (b) Change in concentration of aqueous species with H_2 and NH_3

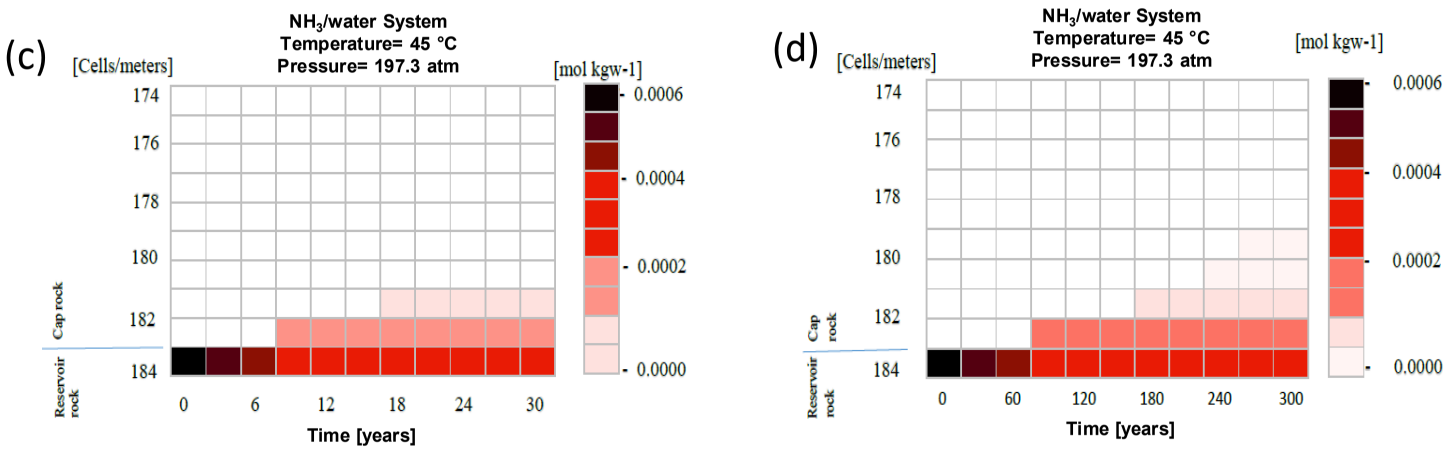

Figure 5 Diffusion of NH_3 through sealing rock after (c) 30 years (d) 300 years

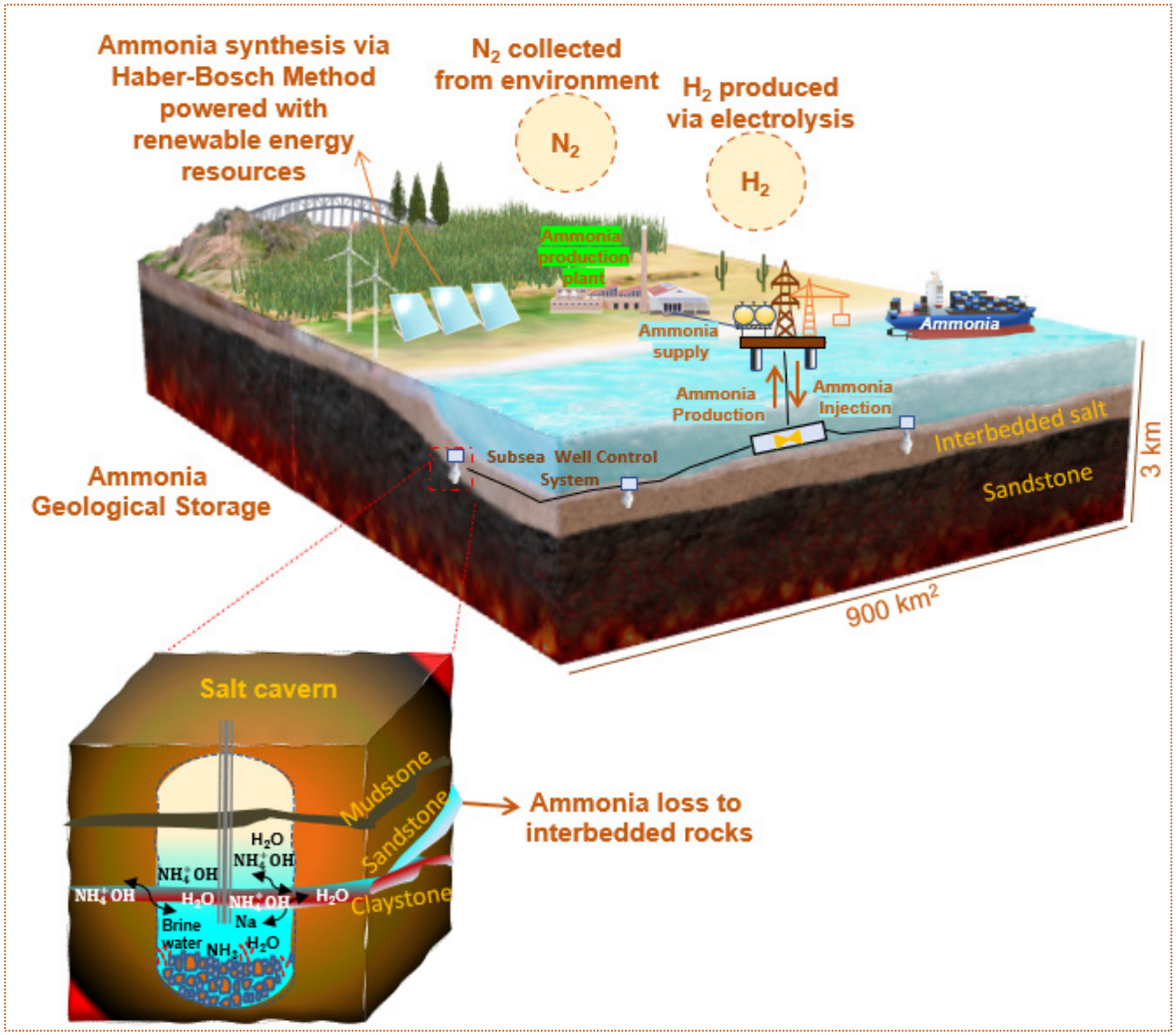

Figure 6 Surface and subsurface activities used for the production, geological storage and utilization of ammonia as an energy source. This figure also illustrates the operational challenges associated with ammonia storage in salt caverns.

Supplementary Information

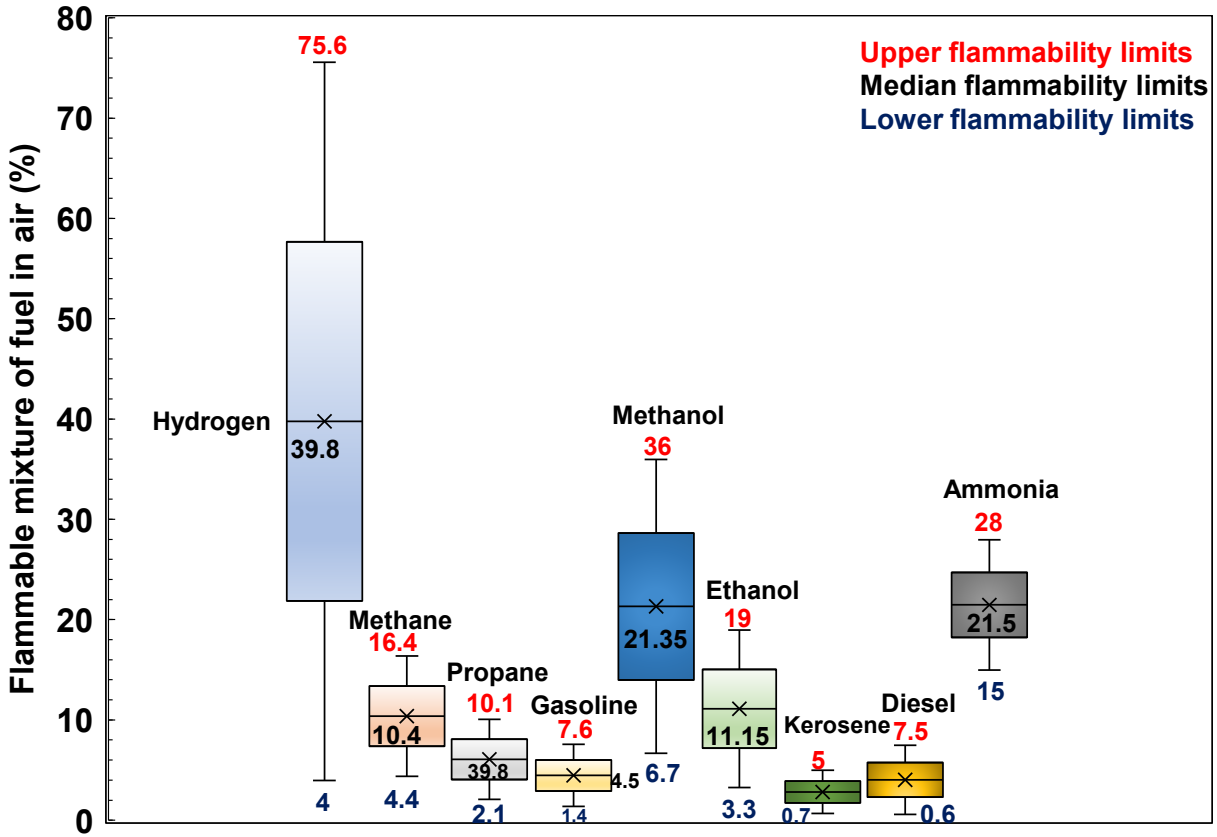

Figure S1 Upper and lower flammability limits of different fuels (EngineeringTool, 2022; Flammability, 2022; Mazloomi and Gomes, 2012)

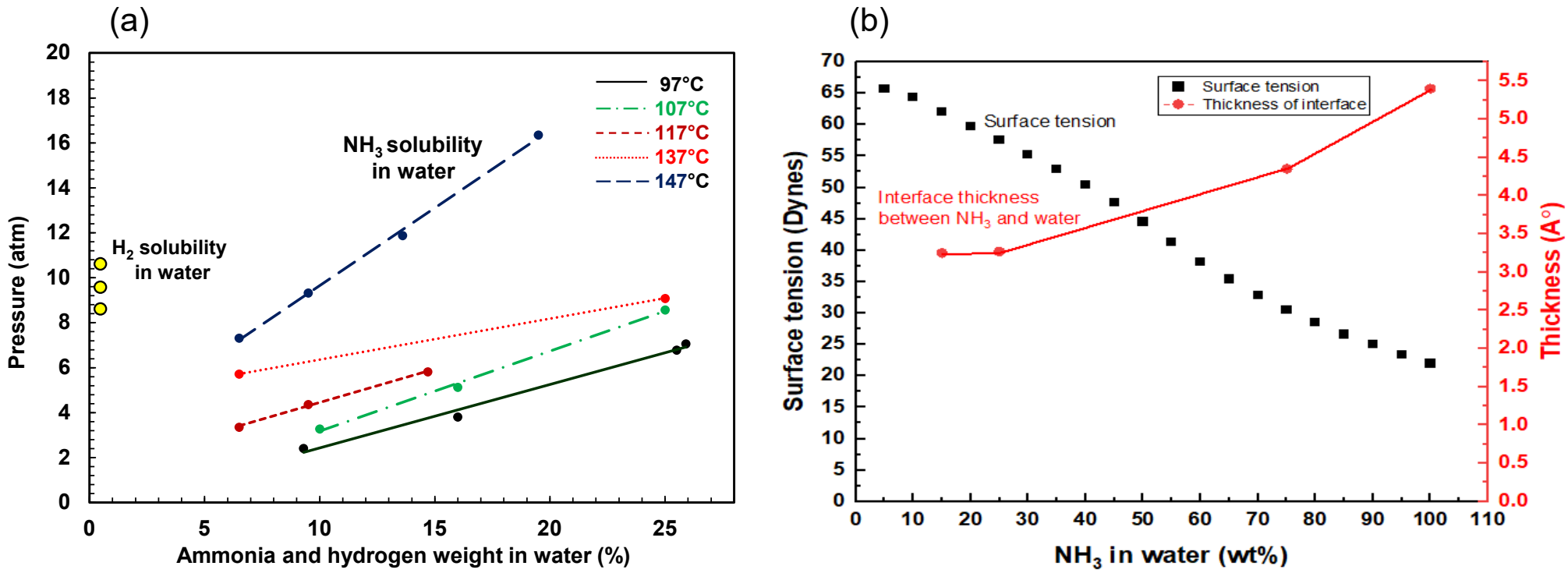

Figure S2 (a) Ammonia and hydrogen weight % in water. The weight percent of ammonia is significantly higher than the percentage of hydrogen in water (Clifford and Hunter, 2002). This indicates that ammonia has highest solubility (<25%) due to its high density at pressure (6.9 atm) and temperature (97 °C) when compared with the H_2 weight percentage (~0.001%), calculated using the Valderrama−Patel−Teja (VPT) equation of state (Hassanpouryouzband et al., 2019). (b) Surface tension and interface thickness of NH_3 water solution at ambient temperature and pressure (Paul and Chandra, 2005; Ware, 1928).

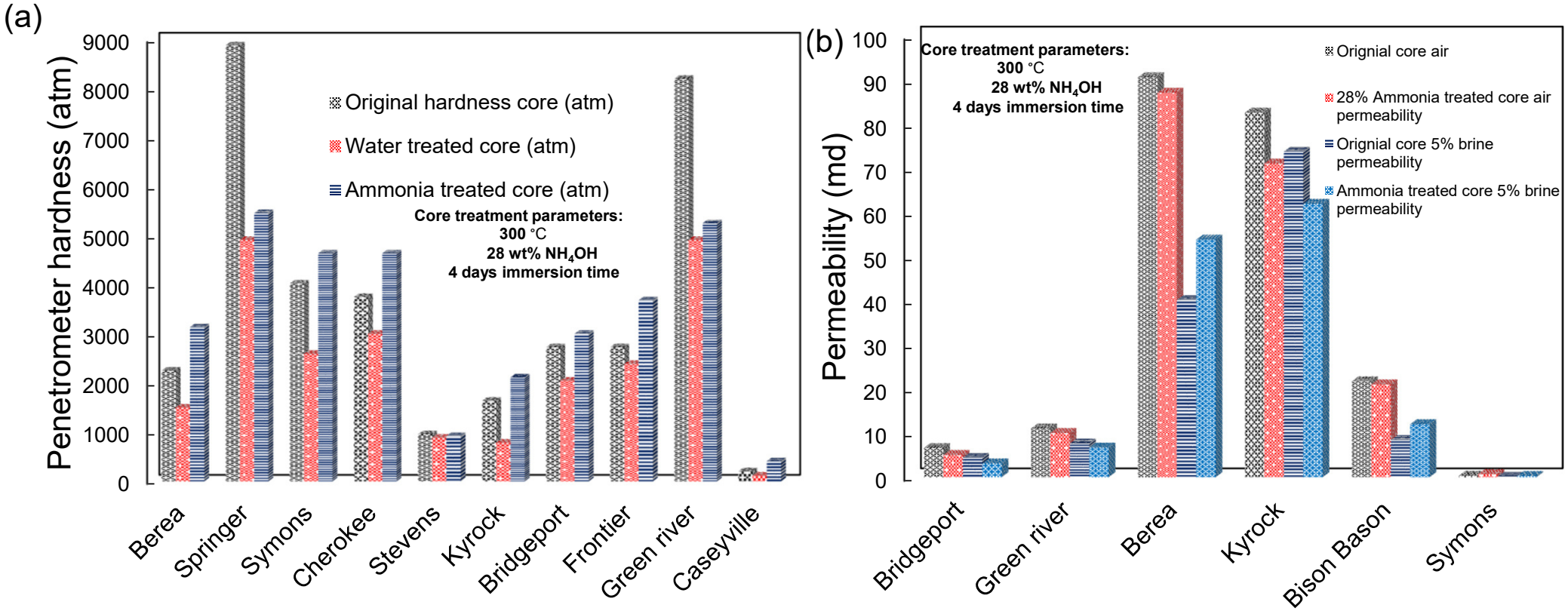

Figure S3 (a) Comparison of sandstone hardness values following treatment with water and ammonia (b) Comparison of sandstone permeability values following treatment with water and ammonia. Results indicate that rock permeability slightly decreases in ammonia treated rocks in comparison to control samples. Permeability significantly reduces in the 5% brine treated samples (Day and Huitt, 1967).

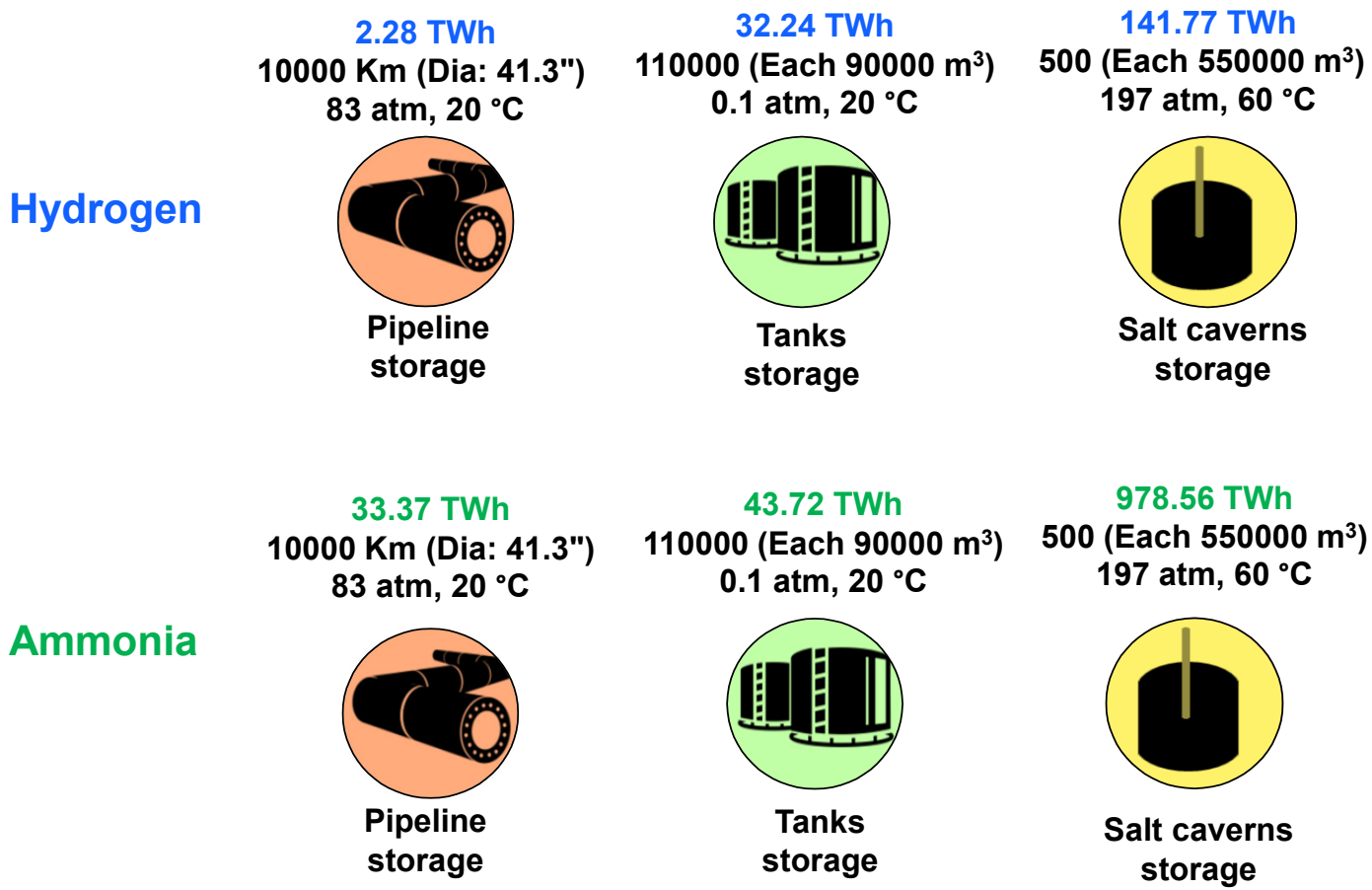

Figure S4 Comparison of hydrogen and ammonia storage capacity values. Figure shows that ammonia has a significantly higher storage capacity when compared to hydrogen. Energy storage capacity calculated using the technique detailed in (Aftab et al., 2022; Hassanpouryouzband et al., 2021 Caglayan et al., 2020;). However, cushion gas volume and cushion gas expansion factors were not considered in the calculations for salt caverns.

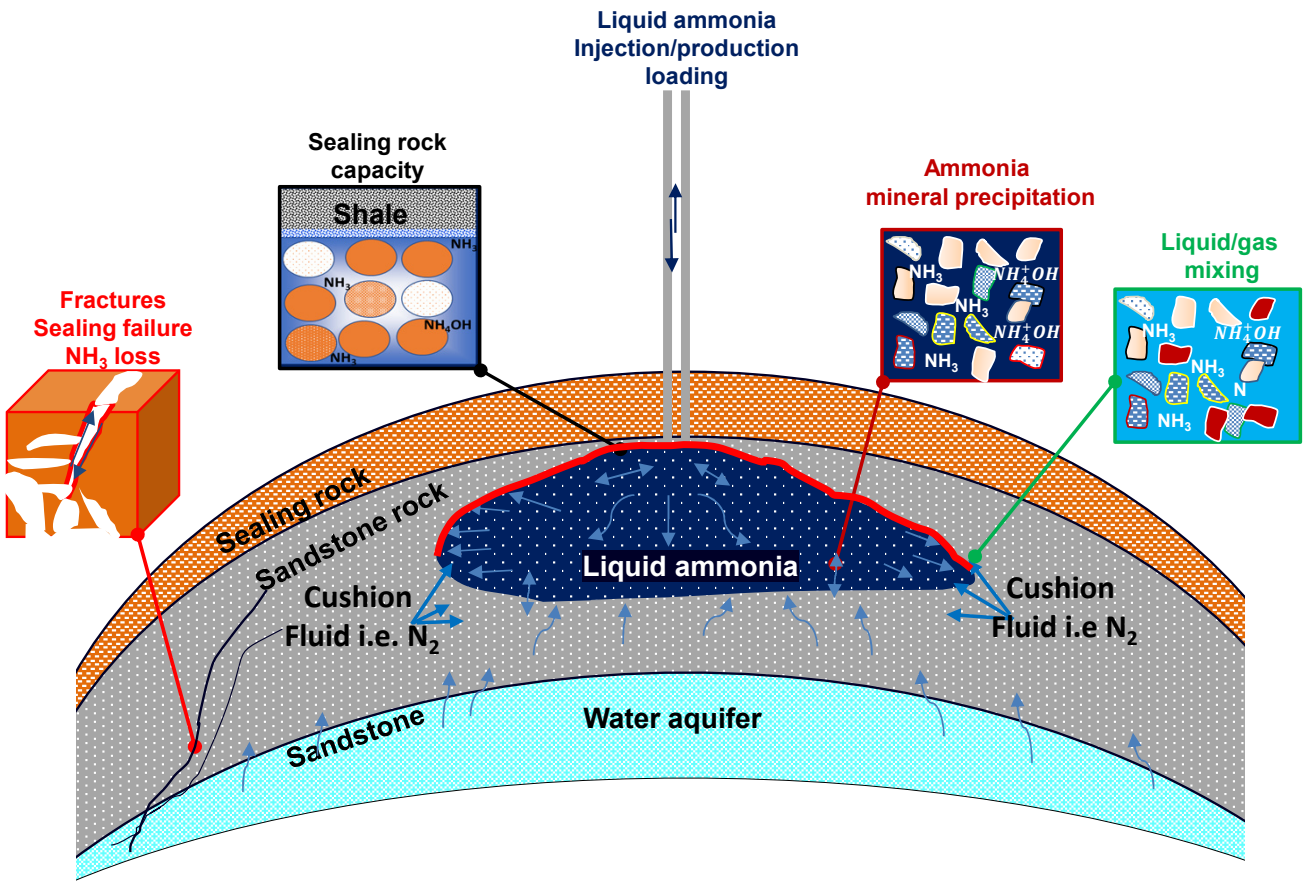

Figure S5 Influences of sealing and fracture failures on geological ammonia storage. Figure illustrates that liquid ammonia may initiate solubility trapping in porous media. Estimates suggest that capillary trapping would be a rare event. However, further numerical and experimental investigations are required to better understand the geological storage challenges in sedimentary reservoir rocks.

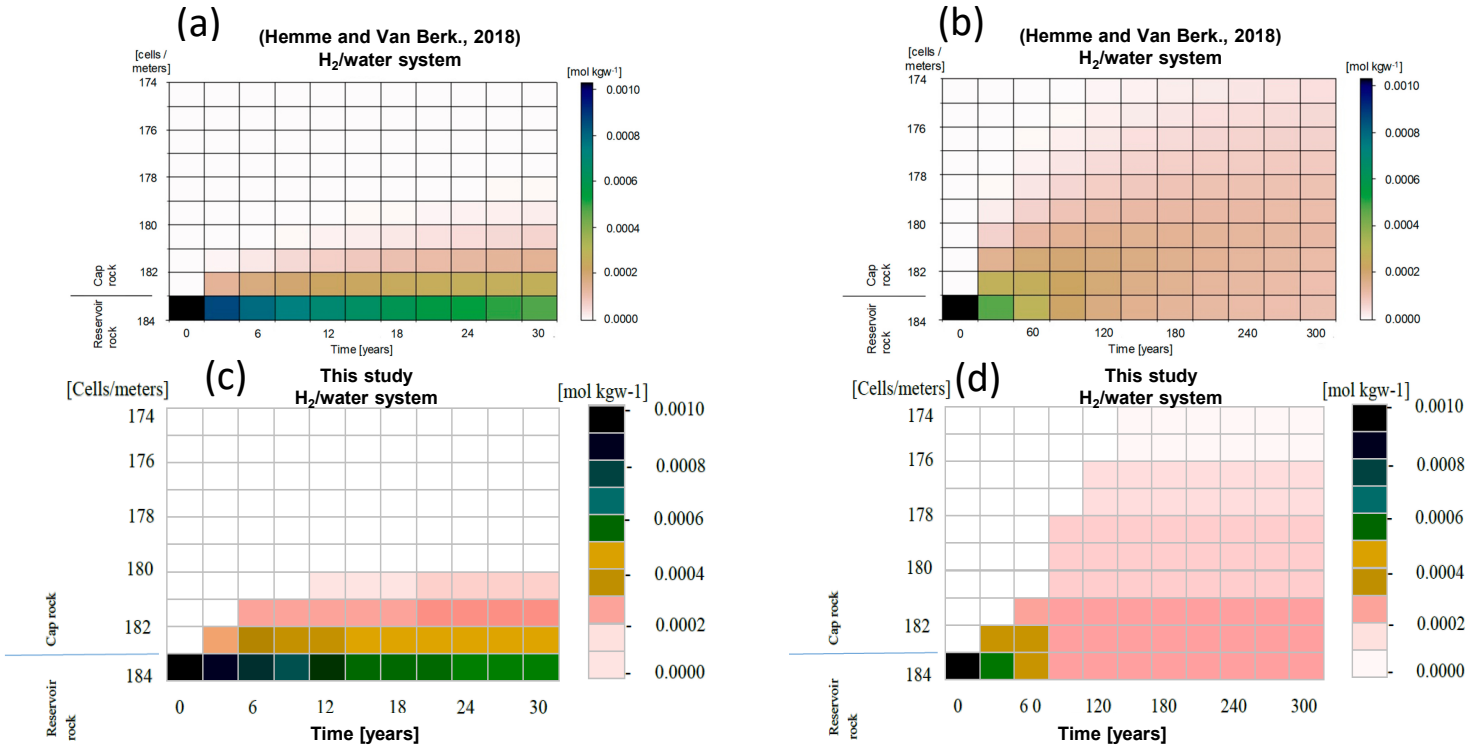

Figure S6 Diffusion of H_2 through sealing rock (a) 30 years (b) 300 years (Hemme and Van Berk., 2018). We have determined diffusion of H_2 through sealing rock after (c) 30 years (d) 300 years.

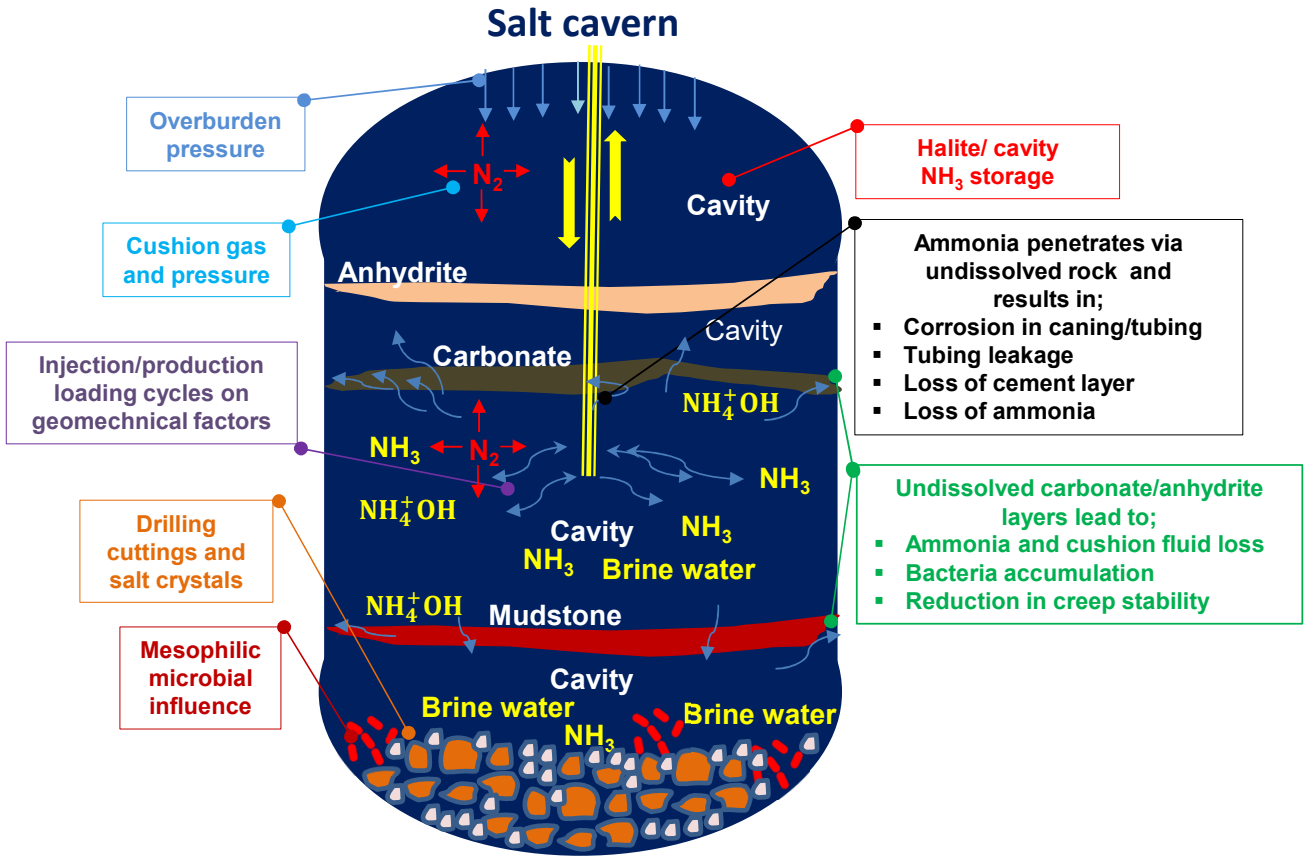

Figure S7 Schematic of ammonia geological storage in a salt cavern. Overburden pressure and injection/production cycles could influence the creep stability of the cavern which may result in geomechnical challenges. Salt caverns constructed in interbedded salt deposits may contain undissolved rock layers or fillings and lead to ammonia loss.

References

Aftab, A., Hassanpouryouzband, A., Xie, Q., Machuca, L.L. and Sarmadivaleh, M., 2022. Toward a Fundamental Understanding of Geological Hydrogen Storage. Industrial & Engineering Chemistry Research, 61(9): 3233-3253.

Back, S., & Jung, Y. (2016). On the mechanism of electrochemical ammonia synthesis on the Ru catalyst. Physical Chemistry Chemical Physics, 18(13), 9161-9166.

Baltrusaitis, J. (2017). Sustainable ammonia production. ACS Sustainable Chemistry & Engineering, 5(11), 9527-9527.

Caballero, L. C., Thornburg, N. E., & Nigra, M. M. (2022). Catalytic ammonia reforming: alternative routes to net-zero-carbon hydrogen and fuel. Chemical Science, 13(44), 12945-12956.

Caglayan, D. G.; Weber, N.; Heinrichs, H. U.; Linßen, J.; Robinius, M.; Kukla, P. A.; Stolten, D., Technical potential of salt caverns for hydrogen storage in Europe. International Journal of Hydrogen Energy 2020, 45, (11), 6793-6805.

Day, J.J. and Huitt, J., 1967. Laboratory study of rock softening and means of prevention during steam or hot water injection. Journal of Petroleum Technology, 19(05): 703-711.

EngineeringTool, 2022. Explosive concentration limits. https://www.engineeringtoolbox.com/explosive-concentration-limits-d_423.html. Assesed on 11th June.

Flammability, 2022. Gases - Explosion and Flammability Concentration Limits. https://www.engineeringtoolbox.com/explosive-concentration-limits-d_423.html. Assessed on April 16th 2022.

Hassanpouryouzband, A., Farahani, M.V., Yang, J., Tohidi, B., Chuvilin, E., Istomin, V. and Bukhanov, B., 2019. Solubility of flue gas or carbon dioxide-nitrogen gas mixtures in water and aqueous solutions of salts: Experimental measurement and thermodynamic modeling. Industrial & Engineering Chemistry Research, 58(8): 3377-3394.

Hemme, C. and Van Berk, W., 2018. Hydrogeochemical modeling to identify potential risks of underground hydrogen storage in depleted gas fields. Applied Sciences, 8(11): 2282.

Liu, Q., Su, P. C., & Chan, S. H. (2022). Wet-air co-electrolysis in high-temperature solid oxide electrolysis cell for production of ammonia feedstock. International Journal of Hydrogen Energy.

Mazloomi, K., & Gomes, C. (2012). Hydrogen as an energy carrier: Prospects and challenges. Renewable and Sustainable Energy Reviews, 16(5), 3024-3033.

Mogensen, M. B., Chen, M., Frandsen, H. L., Graves, C., Hansen, J. B., Hansen, K. V., ... & Sun, X. (2019). Reversible solid-oxide cells for clean and sustainable energy. Clean Energy, 3(3), 175-201.

Paul, S. and Chandra, A., 2005. Liquid-vapor interfacial properties of water-ammonia mixtures: Dependence on ammonia concentration. The Journal of chemical physics, 123(17): 174712.

Sartbaeva, A., Kuznetsov, V. L., Wells, S. A., & Edwards, P. P. (2008). Hydrogen nexus in a sustainable energy future. Energy & Environmental Science, 1(1), 79-85.

Wang, M., Khan, M. A., Mohsin, I., Wicks, J., Ip, A. H., Sumon, K. Z., ... & Kibria, M. G. (2021). Can sustainable ammonia synthesis pathways compete with fossil-fuel based Haber–Bosch processes?. Energy & Environmental Science, 14(5), 2535-2548.

Ware, G.C., 1928. Surface tension of liquid ammonia and adsorption studies at its liquid vapor interface. Master of Science Thesis. Kansas State Agricultural College.

Supplementary Information

Unlocking Geological Hydrogen Storage with Ammonia: An Effort for Net-Zero Future

Adnan Aftab *Curtin University, Australia*
King Abdullah University of Science & Technology, Saudi Arabia

*Corresponding authors E-mail: *adnanaftab1199@gmail.com*; *adnan.aftab@curtin.edu.au*

The software includes an algorithm for one dimensional transport setup to determine the effect of diffusivity and dispersion in a dual porosity medium. Additionally, inverse modeling features identify the hydrogeochemical reaction in the formation with respect to time. Salt cavern and reservoir rock setup and factors including reservoir conditions, injection scenario, mass transport reaction, and grid resolution are provided in the supplementary information.

Salt cavern setup

NH_3 occurs in a gas state at ambient temperature and pressure. Once NH_3 will be injected into the salt cavern it changes from gas to liquid phase. Thus, brine water available in the cavern is in equilibrium with the liquid ammonia. We assume typical conditions of salt cavern i.e., temperature =44.8 °C and pressure =197.3 atm. Salt caverns are typically consisting of halite and anhydrite salts. Thus, we determine the saturation index (SI) of the solutions NH_3/Halite and NH_3/Anhydrite at variable concentrations of NH_3 (0-75 wt%), the constant pressure and temperature in the course of the reaction time. The SI data evaluates supersaturation, equilibrium, and undersaturation behavior of halite and anhydrite with NH_3/water solution. These data help us to understand NH_3 compatibility with the salts in the salt cavern to determine the effect of precipitations and contaminant problems. Moreover, NH_3 dissociates into NH_4^+ and NH_4^+OH when mixes in water and water/salt solution. The mechanism can moist NH_3 and affect the quality of stored NH_3. Thus,

we determine NH_3 transforms into NH_4^+ or NH_4^+OH at variable concentrations of NH_3 and the geo storage conditions. We have used data from phreeqc.dat file. Moreover, the equilibrium phase, mass action equations, and other related data are present in the previous studies (Parkhurst and Appelo, 2013; Hemme and Van Berk, 2018).

Reservoir rock setup

We use PHREEQC version 3 (Parkhurst & Appelo, 2013) and a Python code (Waskom, 2014) to simulate the underground ammonia storage in the depleted gas reservoir. PHREEQC simulates the equilibrium reaction between ammonia, rock, and water, as well as the kinetic reaction for solubility and diffusivity. It provides the data for the transport of ammonia from reservoir rock to caprock. We model the transport of NH_3 using PHREEQC model for transport modeling and plot 1D transport grid graphs using a Python-based plot code by (Waskom, 2014). The complete code and reference are provided in the supplementary information. The model considers the kinetic reaction diffusive transport of aqueous species in the NH_3 storage system and takes into account the thermodynamic interactions between ammonia and rock water. Table S1 provides equilibrium constants, equilibrium reaction, and equilibrium phases data.

Table S1 Equilibrium constants, equilibrium reaction, and equilibrium phases in the model (Parkhurst & Appelo, 2013; Hemme and Van Berk, 2018).

Equilibrium Phase	Equilibrium Reaction	log K at 25 °C, 0.98 atm
K-feldspar	$KAlSi_3O_8 + 8H_2O = K^+ + Al(OH)_4^- + 3H_4SiO_4$	−20.573
Albite	$NaAlSi_3O_8 + 8H_2O = Na^+ + Al(OH)_4^- + 3H_4SiO_4$	−18.002
Kaolinite	$Al_2Si_2O_5(OH)_4 + 6H^+ = H_2O + 2H_4SiO_4 + 2Al^{3+}$	7.435

Quartz	$SiO_2 + 2H_2O = H_4SiO_4$	3.98
Calcite	$CaCO_3 = CO_3^{2-} + Ca^{2+}$	8.48
Pyrite	$FeS_2 + 2H^+ + 2e^- = Fe^{2+} + 2HS^-$	−18.479
Illite	$K_{0.6}Mg_{0.25}Al_{2.3}Si_{3.5}O_{10}(OH)_2 + 11.2H_2O = 0.6K^+ + 0.25Mg^{2+} + 2.3Al(OH)^{4-} + 3.5H_4SiO_4 + 1.2H^+$	−40.267
Dawsonite	$NaAlCO_3(OH)_2 + 3H^+ = Al^{3+} + HCO_3^- + Na^+ + 2H_2O$	4.35
Mackinawite	$FeS + H^+ = Fe^{2+} + HS^-$	−4.648
Dolomite	$CaMg(CO_3)_2 = Ca^{2+} + Mg^{2+} + 2CO_3^{2-}$	−17.09
Nahcolite	$NaHCO_3 = HCO_3^- + Na^+$	−0.11
Anhydrite	$CaSO_4 = Ca^{2+} + SO_4^{2-}$	−4.39
Halite	$NaCl = Cl^- + Na^+$	1.570
Gypsum	$CaSO_4 \cdot 2H_2O = Ca^{2+} + SO_4^{2-} + 2H_2O$	−4.58
Sulfur (element)	$S + 2H^+ + 2e^- = H_2S$	4.882
Barite	$BaSO_4 = Ba^{2+} + SO_4^{2-}$	−9.97
Goethite	$FeOOH + 3H^+ = Fe^{3+} + 2H_2O$	−1.0
NH_4^+	$NH_3 + H^+$	-9.252
$NH_{3(g)}$	$NH_3 = NH_3$	1.796
$H_{2(g)}$	$H_2 = H_2$	−3.1050
$CO_{2(g)}$	$CO_2 = CO_2$	−1.468
$CH_{4(g)}$	$CH_4 = CH_4$	−2.8502
$H_2S_{(g)}$	$H_2S = H^+ + HS^-$	−7.9759

$N_{2(g)}$	$N_2 = N_2$	−3.1864

The model predicts changes in the porosity and partial pressure of the storage gas and evaluates the effects of NH_3 storage on the composition of the aqueous solution, mineralogy of the reservoir, and cap rocks. We update PHREEQC program of the previous study (Hemme and Van Berk, 2018) with some new modifications to simulate the equilibrium reactions as mentioned in the supplementary material.

The model utilizes the mass action law to calculate equilibrium, taking into account all species of reservoir rock, including Al, Ba, C, Ca, Cl, Fe, K, Mg, N, Na, S, and Si and their equilibrium. The equilibrium phases, mass action equations, and equilibrium constants in the model are available in the supplementary material. For more information about PHREEQC, readers can refer to (Parkhurst & Appelo, 2013). It is important to note that this section provides a concise overview of the modeling tools and techniques used in the present numerical simulation work for underground NH_3 storage (Parkhurst & Appelo, 2013).

Reservoir conditions: The model assumes a depleted gas field thats divided into three columns (i.e. Cap rock, reservoir rock and underlying rock) in which each column contains a different temperature and different pressures for underground storage of NH_3. The reservoir rock consists of sandstone with a porosity of 10%. The caprock consists of shale having a porosity of 5%. The reservoir depth is 4881ft. The initial reservoir Condition is set to a mixture of water and ammonia.

We apply the Cauchy boundary condition which is set to a closed system where the mass of the reservoir remains constant (Hemme and Van Berk, 2018).

Injection scenario: NH_3 is injected into the reservoir rock with different concentrations (i.e., 5 wt%, 15 wt%, 25 wt%, 50 wt%) to measure the solubility, and PH in the different systems at different pressures and temperatures. The initial reservoir brine is assumed moreover NH_3 to be in equilibrium with residual gas from the previous natural gas reservoir. As NH_3 is injected, the available brine becomes saturated with NH_3 and the initial reservoir brine is displaced. The equilibrium constants for the reaction involving ammonia in water can be obtained from the PHREEQC database.

Mass transport and reaction: The model assumes that NH_3 dissolves into the cap rock brine and diffuses through the cap rock brine. The reactive mass transport model considers the interaction between NH_3, the surrounding rock, and the brine, including possible reactions between NH_3 and minerals in the rock or brine. The simulation is carried out for 30 years to study the long-term behavior of the system. The NH_3 reaction rate for diffusion is the function of the concentration of ammonia and the equilibrium constant. The diffusion coefficient value of NH_3 is $2.28 \times 10^{9} m^{2}\ s^{-1}$ taken from the PHREEQC database.

Grid resolution: The model is discretized into a 1D column with a different number of cells, each with a different height. The cap rock is represented by the first 182 cells, with different pressures and temperatures. The reservoir rock cells are from 183 to 850. The underlying rock cells are from 851 to 1488. The grid resolution is chosen based on a balance between computational efficiency and the need to capture the relevant spatial scales of the system. It is also valid through a different height of cell as (2,4,6)m height and different parameters.

Software and parameters: The simulation is carried out using the reactive transport software PHREEQC. which can model a range of geochemical and reactive mass transport processes. Parameters such as mineralogy, porosity, and permeability are based on available data from the reservoir and cap rock and may need to be adjusted or refined based on further analysis or experimental data.

Key points regarding ammonia toxicity and safety measures

We have provided critical points regarding NH_3 toxicity in the supplementary information. Table S2 enlists the variety of NH_3 concentrations and its toxicity effects on the human health.

- The time weighted average (8 hours/day and 40 hours/week) for NH_3 is 25 ppm (18 mg/m^3) and short-term exposure limit (15 min average) is 35 ppm (27 mg/m^3) according to American Conference of Governmental Industrial Hygienists, Occupational Safety and Health Administration, and National Institute for Occupational Safety and Health.
- Liquid NH_3 can accumulate in the lungs and result in a life-threatening condition. Early symptoms of continuous NH_3 inhalation include tightness in the chest and breathing difficulties.
- NH_3 is corrosive and can cause burns and permanent scarring. Severe symptoms include skin stiffness and burning. The skin can appear yellow, waxy, or white and blistered.
- NH_3 vapors can burn or irritate eyes and cause permanent blindness. Direct contact with eyes may cause permanent damage.
- Aqueous ammonia transforms into ammonia gas when released in the atmosphere. The prolonged heat exposure to NH_3 tanks may cause fire incidents and lead to rocketing and violent rupturing.

- However, the effects of NH_3 on teratogenicity / embryotoxicity, mutagenicity, and reproductive toxicity are unknown.

Table S2 Ammonia concentrations and toxicity effects (CCOHS, 2022; EnviroMed, 2022; NLM, 2022a).

NH_3 concentration in air (ppm)	Retention medium & percent	Exposure time (h)	Effects
24	NA	2 to 6	• Nose and throat irritant
25	30 %	NA	• NH_3 has observed in blood
32	NA	24	• The level in blood increases.
30	NA	0.16	• Mild irritant
50	NA	0.16	• Moderate irritant
72-134	NA		• Irritate nose and throat irritation
57-500	83 to 92%	0.03	• High nasal retention • Upper respiratory tract retention • Pharyngeal irritation
310-1157	NA	0.8	• Exposure irritation • High increase in blood NH_3 level
1500	NA	NA	• The fluid accumulation in the lungs • Potential for fatal pulmonary edema. • Pulmonary edema may be asymptotic

References

Arnold, J.H., 1930. Studies in diffusion. II. A kinetic theory of diffusion in liquid systems. Journal of the American Chemical Society, 52(10): 3937-3955.

Carlson, T., 1911. THE DIFFUSION OF OXYGEN IN WATER. Journal of the American Chemical Society, 33(7): 1027-1032.

CCOHS, 2022. OSH Answers Fact Sheets Ammonia. https://www.ccohs.ca/oshanswers/chemicals/chem_profiles/ammonia.html. Assessed on 11th June

Council, N.R. and Levels, C.o.A.E.G., 2008. Ammonia Acute Exposure Guideline Levels, Acute Exposure Guideline Levels for Selected Airborne Chemicals: Volume 6. National Academies Press (US).

Davidson, J., 1957. The determination of diffusion coefficient for sparingly soluble gases in liquids. Trans. Instn Chem. Engrs., 35: 51-60.

EnviroMed, 2022. What are the hazards of working with Ammonia? https://enviromed.ca/index.php?id_cms=28&controller=cms. Assessed on 11th June.
Green, D.W. and Perry, R.H., 2008. Perry's chemical engineers' handbook. McGraw-Hill Education.
Grilly, E., 1951. The Vapor Pressures of Hydrogen, Deuterium and Tritium up to Three Atmospheres1. Journal of the American Chemical Society, 73(2): 843-846.
Huber, M.L., Perkins, R.A., Laesecke, A., Friend, D.G., Sengers, J.V., Assael, M.J., Metaxa, I.N., Vogel, E., Mareš, R. and Miyagawa, K., 2009. New international formulation for the viscosity of H 2 O. Journal of Physical and Chemical Reference Data, 38(2): 101-125.
Kapeghian, J.C., Mincer, H.H., Jones, A.B., Verlangieri, A.J. and Waters, I.W., 1982. Acute inhalation toxicity of ammonia in mice. Bulletin of environmental contamination and toxicology, 29(3): 371-378.
Laesecke, A. and Muzny, C.D., 2017. Reference correlation for the viscosity of carbon dioxide. Journal of physical and chemical reference data, 46(1): 013107.
Leachman, J.W., Jacobsen, R.T., Penoncello, S. and Lemmon, E.W., 2009. Fundamental equations of state for parahydrogen, normal hydrogen, and orthohydrogen. Journal of Physical and Chemical Reference Data, 38(3): 721-748.
Monogenidou, S., Assael, M.J. and Huber, M.L., 2018. Reference Correlation for the Viscosity of Ammonia from the Triple Point to 725 K and up to 50 MPa. Journal of physical and chemical reference data, 47(2): 023102.
Moradi, H., Azizpour, H., Bahmanyar, H., Mohammadi, M. and Akbari, M., 2020. Prediction of methane diffusion coefficient in water using molecular dynamics simulation. Heliyon, 6(11): e05385.
Speight, J.G., 2017. Lange's Handbook of Chemistry. McGraw-Hill Education, New York.